

FAST RELIABLE PRICING AND CALIBRATION OF THE ROUGH HESTON MODEL

SVETLANA BOYARCHENKO, MARCO DE INNOCENTIS AND SERGEI LEVENDORSKII

ABSTRACT. The paper is an extended and modified version of the preprint S.Boyarchenko and S.Levendorskii “Correct implied volatility shapes and reliable pricing in the rough Heston model”. We combine a modification of the Adams method with the SINH-acceleration method S. Boyarchenko and S. Levendorskii (IJTAF 2019, v. 22) of Fourier inversion (iFT) to price vanilla options under the rough Heston model. For moderate or long maturities and strikes near spot, thousands of prices are computed in several milliseconds (ms) in MATLAB on a Mac with moderate specs, with relative errors $\lesssim 10^{-4}$. Even for options close to expiry and far-OTM, the pricing takes a few tens or hundreds of ms.

We show that, for the calibrated parameters in El Euch and Rosenbaum (Math. Finance 2019, v. 29), the model implied vol surface is much flatter and fits the market data poorly; thus the calibration in *op. cit.* is a case of “ghost calibration” (M. Boyarchenko and S. Levendorskii, Quant. Finance 2015, v. 15): numerical error and model specification error offset each other, creating an apparently good fit that vanishes when a more accurate pricer is used. We explain how such errors arise in popular iFT implementations that use fixed numerical parameters, yielding spurious smiles/skews, and provide numerical evidence that SINH acceleration is faster and more accurate than competing methods. Robust error control is ensured by a general Conformal Bootstrap principle that we formulate; the principle is applicable to many Fourier-pricing methods. We outline how this principle and our method enable accurate calibration procedures that are hundreds of times faster than approaches commonly used in the industry.

Disclaimer: The views expressed herein are those of the authors only. No other representation should be attributed.

KEY WORDS: rough Heston model, fractional Adams method, Fourier transform, sinh-acceleration, CM method, COS method, Lewis method, calibration, conformal bootstrapping principle
MSC2020 CODES: 60-08, 60E10, 60G10, 60G22, 65C20, 65D30, 65G20, 91G20, 91G60

CONTENTS

1. Introduction	2
2. Rough Heston model and its Markovian approximation	8
2.1. Formulas for the characteristic function	8
2.2. Asymptotics of $\phi(\xi, \tau) := g_1(\xi, \tau) + vg_2(\xi, \tau)$ as $\tau \rightarrow \infty$	9
2.3. A generalization of (2.10)	10
2.4. Markovian approximation of rough volatility	11
3. Fractional Adams method and its modification	12

S.B.: Department of Economics, The University of Texas at Austin, 2225 Speedway Stop C3100, Austin, TX 78712–0301, sboyarch@utexas.edu

M.I.: Deutsche Bank, 21 Moorfields, London, EC2Y 9DB. Email address: marcdein@gmail.com

S.L.: Calico Science Consulting. Austin, TX. Email address: levendorskii@gmail.com.

3.1. Prediction-correction method (a.k.a. Adams method)	12
3.2. BL modification of Adams method	12
4. Several methods for Fourier inversion	15
4.1. Flat iFT and simplified trapezoid rule	15
4.2. Carr-Madan method	17
4.3. Gaussian quadratures	17
4.4. COS method [35]	20
4.5. SINC method	20
4.6. Flat iFT-BM and Flat iFT-NIG methods	20
4.7. Summation by parts in the infinite trapezoid rule	21
4.8. SINH-acceleration	22
4.9. Ad-hoc bound for ϕ and choice of N in the rough Heston model	23
4.10. Conformal bootstrap principle	24
5. Numerical examples	25
5.1. Comparison of the efficiency of different methods for pricing in the Heston model	25
5.2. Performance in “good regions” of the (K, T) -plane	26
5.3. Examples of incorrect shapes	27
6. Fast pricing	28
6.1. Pricing algorithms	28
6.2. Calibration pricer	28
6.3. Performance times	28
7. Calibration results	30
7.1. Calibration using SINH-CB	30
7.2. Calibration pitfalls	32
8. Conclusion	33
References	35
Appendix A.	38
A.1. Grids depending on ξ	38
Appendix B. Pseudo-code implementation of the BL modification of the Adams method	39
Appendix C. Benchmark pricing algorithm	40
C.1. Choice of ω grid	41
C.2. Calculation of $F(\omega; X)$	41
C.3. Calculation of the benchmark prices $V(T, K; \omega)$	41
C.4. Calculation of $\omega(X)$	42
Appendix D. Pricing algorithm for the Markovian approximation (BL2)	43
Appendix E. Additional tables and figures	45

1. INTRODUCTION

Starting with the celebrated Heston model [43], affine models have become one of the most popular classes of stochastic volatility models, term structure models, and models in FX. The popularity is due to the fact that the characteristic function in an affine model can be explicitly calculated solving an associated system of generalized Riccati equations [31], hence, the Fourier

transform technique allows one to express prices of options of the European type as oscillatory integrals. However, despite their analytical convenience, models based on classical affine diffusions such as Heston have well-documented limitations in reproducing key features of observed implied volatility surfaces. In particular, these models are unable to capture adequately the pronounced short-maturity steepness of implied volatility smiles – a feature consistently observed in equity and FX markets. In response to these shortcomings, a new class of models, that of *rough volatility* models, has been proposed. These models replace the standard Brownian Motion (BM) drivers of volatility with fractional processes characterised by a Hurst index $H \in (0, 1/2)$. Examples of how the model provides a good fit of steep smiles at very short expiries can be found in Figure 5 in section 7.

Empirical evidence presented by Gatheral, Jaisson, and Rosenbaum [41] demonstrated that, at the time, the log-volatility of financial assets behaved as a fractional Brownian motion with $H \approx 0.1$, both in historical and implied volatility data. This low Hurst index implies a “rough” volatility path that is far less smooth than Brownian motion, leading to stronger short-term memory and more accurate modelling of the volatility clustering and bursts which are often observed in financial markets. For various aspects of rough volatility models, see [8, 41, 49, 34, 38, 38, 37, 39, 40, 9] and the bibliographies therein. The theoretical elegance of rough volatility models comes at a significant practical cost. The volatility process, driven by a fractional Brownian motion (fBM), is neither a Markov process nor a semimartingale. Although the characteristic function of the rough Heston model has the standard affine structure, the coefficients are expressed in terms of the solution of a fractional Volterra equation for which no explicit solution is known; its numerical solution is a computationally intensive task. The non-Markovian nature of fBM precludes the use of classical PDE methods and makes simulation costly. Monte Carlo methods for such models are significantly more difficult to implement. A range of Euler schemes have been introduced, enabling simulation of rough paths. In parallel, Markovian approximations [45, 7] have been introduced to approximate rough Heston dynamics through high-dimensional Markovian systems, relying on affine techniques (cf. Section 2.4). These approaches, while representing important progress towards making rough volatility models viable, are still too slow for practical applications¹. Furthermore, the reliance on numerical Fourier inversion for pricing introduces its own subtle but critical risks. As demonstrated by M. Boyarchenko and Levendorskii [11], naive applications of popular Fourier methods with fixed, non-optimal parameters can lead to *ghost calibration*. In this phenomenon, numerical inaccuracies of the pricing algorithm systematically offset the model’s specification errors, producing a fallacious, yet seemingly excellent, fit to market data with incorrect model parameters and a distorted implied volatility surface. Conversely, the correct model may be ruled out simply because, at the true parameters, numerical error dominates: *sundial calibration* [51]: a sundial never shows midnight².

Avoiding these pitfalls is paramount for reliable calibration and risk management, and it necessitates a numerical method that is not only fast but also fundamentally robust. This paper introduces such a method (dubbed SINH-CB method: *SINH-acceleration with Conformal*

¹See Table 8 in section 6.3.5, and [7, Sect. 4.1]. Reported times correspond to the full algorithm of [7], covering both the Riccati solver and the Fourier inversion steps.

²See section 7.2 for an example of ghost/sundial calibration to market data.

Bootstrapping). We discuss several advantages on the SINH-CB method for practical implementations in sect. 8; we hope that the method will be instrumental in resolving the following recent controversy. In several empirical publications, e.g., [59, 48], the authors find that rough volatility models do not reproduce the volatility surface accurately and certain affine diffusion models perform the task better. In particular, one of the general conclusions in the abstract of [48] is that the skew of rough volatility models “increases too fast for short maturities and decays too slowly for longer maturities”. In the paper, we demonstrate that incorrect shapes of implied volatility curves and surfaces are often caused *not* by a choice of an incorrect model but by a choice of an inaccurate numerical method (the pricer) used in the calibration procedure. Moreover, as discussed in section 6.3, our new method is so fast that it is expected to run in a few milliseconds or tens of milliseconds, when compiled as native code on a high-performance computing system (without GPU acceleration).

The main elements of the SINH-CB method are as follows. Let Φ be the (conditional) characteristic function of the Heston model or rough Heston model (see (2.3) below), and let the riskless rate r be constant. Then, with an appropriate choice of the line of integration, the price of the put, call or covered call option on non-dividend paying underlying can be represented in the form

$$(1.1) \quad V(S_0, K; T) = -\frac{Ke^{-rT}}{\pi} \operatorname{Re} \int_{\operatorname{Im} \xi = \omega_1} \frac{e^{i\xi \ln(S_0/K)} \Phi(\xi, T)}{\xi(\xi + i)} d\xi.$$

In the Heston model and rough Heston model, the integral can be calculated sufficiently accurately for applications using the simplified trapezoid rule (Flat iFT - flat inverse Fourier transform method) with 200-400 terms if the time to maturity is not too short. The reason is the exponential decay of the discretization error of the infinite trapezoid rule as the function of $1/\zeta$, where ζ is the step, if the integrand is analytic in a strip $S_{(a,b)} := \{\xi \mid \operatorname{Im} \xi \in (a,b)\}$ around the line of integration and decays sufficiently fast at ∞ . If T is of the order of several days and/or the option is deep OTM, the integrand decays too slowly and/or strongly oscillates, and Flat iFT may produce large errors. However, in all popular models bar stable Lévy models different from BM, $\Phi(\xi, T)$ admits analytic continuation to a region of the form $\mathcal{U}(\gamma_-, \gamma_+; \mu_+, \mu_-) := i(\mu_+, \mu_-) + (\mathcal{C}_{\gamma_-, \gamma_+} \cup (-\mathcal{C}_{-\gamma_+, \gamma_-}) \cup \{0\})$, where $\mu_- < -1 < 0 < \mu_+$, $\mathcal{C}_{\gamma_-, \gamma_+} := \{\xi \in \mathbb{C} \mid \arg \xi \in (\gamma_-, \gamma_+)\}$. We choose a deformation of the contour of integration into a contour $\mathcal{L}_{\omega_1, b, \omega} := \chi_{\omega_1, b, \omega}(\mathbb{R})$, where the conformal map $\chi_{\omega_1, b, \omega}$ (*sinh-deformation*) is defined by

$$(1.2) \quad \chi_{\omega_1, b, \omega}(y) = i\omega_1 + b \sinh(i\omega + y),$$

and $\omega_1 \in \mathbb{R}$, $b > 0$ and $\omega \in (\gamma_-, \gamma_+)$. The parameters of the deformation are chosen so that in the process of deformation, the contour remains in $\mathcal{U}(\gamma_-, \gamma_+; \mu_+, \mu_-)$, the oscillating factor becomes a fast decreasing one and the poles at $\xi = 0, -i$ are not crossed. The subsequent change of variables $\xi = \chi_{\omega_1, b, \omega}(y)$ makes the integrand a fast decaying one in a strip of the form $S_{(-d, d)}$, hence, the error of the truncation of the infinite sum is easy to control. Fig.1 illustrates the sinh-acceleration. In essentially all cases we tried, an absolute error tolerance of the order of $E - 09$ can be satisfied with 20-60 terms of the simplified trapezoid rule. For the error control, we calculate the prices using two deformations. The probability that the difference of the two weighted sums of the values of the integrand calculated at different nodes on different curves is significantly larger than the difference of either sum and the true price is essentially

zero (assuming that the prior distribution of prices is uniform in the no-arbitrage interval). This is an ad-hoc principle which we call Conformal Bootstrap principle. In applications to option pricing, we use a pair of deformations for OTM puts, and a pair for OTM calls; for a given error tolerance, the step ζ is calculated using a universal prescription. If two prices for calls do not agree well for a chosen N , a small number of additional terms can be easily added, which is a serious advantage as compared with adaptive quadratures. Even simpler, a larger than necessary N^* can be used, and prices calculated with N^* and smaller N compared to make sure that the truncation error is small. The resulting program is only a few lines long, and the block for the evaluation of the parameters $\omega_1, b, \omega, \zeta$ (and N if the rate of decay of $\Phi(\xi, T)$ is known) is likewise only a few lines long. Note that SINH-CB method can be used in all situations where numerical Fourier inversion is applied, and to numerical evaluation of complicated integrals of a different nature. If the domain of analyticity is unknown, we use 2-3 deformations and compare the results as in the case when the domain is known, and, to ensure that in the process of deformation, no pole or singularity has been crossed, calculate the integral using $\omega = 0$.

In the case of the rough Heston model, the characteristic function is calculated by solving the fractional Volterra equation. Typically, the fractional Volterra equation is solved numerically using the fractional Adams method. We improve the accuracy of the evaluation of the characteristic function by using a modification (Modification III in the initial version of the paper) of the fractional Adams method³. Large errors of the Adams method are documented in [25], where the fractional Riccati equation is solved using the asymptotic expansion of the solution near 0 and the Richardson-Romberg extrapolation [58] farther from 0, and the Carr-Madan (CM method) [26] is applied. For the example considered in [25], SINH-CB method is significantly faster and, for options of short maturities, produces more accurate results than the hybrid and CM methods taken together.

Next, we conduct the comparative analysis of methods of Fourier inversion in application to pricing in the rough Heston model [34] and in the Heston model, in order to clearly separate the errors of the Fourier inversion methods and errors of the numerical evaluation of the characteristic function. We demonstrate that for practical applications, adaptive quadratures such as Gauss-Kronrod are sufficiently accurate (albeit less accurate) than some of the methods that we describe in the paper, but too slow. The other popular methods are either too inaccurate, especially for pricing short maturity options and deep OTM options, or lack a reliable procedure for the choice of parameters of the numerical scheme. In the quantitative finance literature, we found a number of examples with incorrect implied volatility curves and surfaces and the ATM skews. Different methods are used in the literature; in essentially all cases, the details of the numerical implementation such as the number of nodes N of the quadrature are not provided. However, the performance of even a good quadrature such as the Gauss-Laguerre quadrature strongly depends on the choice of the parameters. In Table 1, we show the results of pricing using the Gauss-Laguerre and Gauss-Legendre quadratures and SINH-CB method, for the rough Heston model [34] with the parameters

$$(1.3) \quad \alpha = 0.62, \gamma = 0.1, \rho = -0.681, \theta = 0.3156, \nu = 0.331, v_0 = 0.0392,$$

³Accurate calculations of the the log-characteristic function in a host of affine models can be challenging as well if the system of generalized Riccati equations can be solved only numerically - see the analysis in [52].

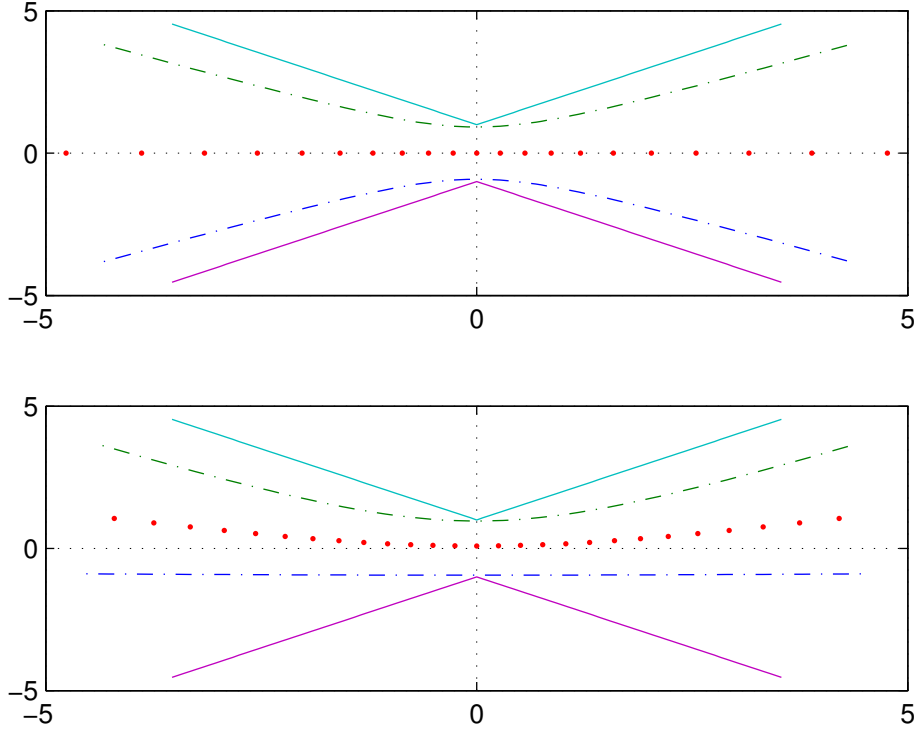


FIGURE 1. Solid lines: boundaries of the domain of analyticity $S_{(-1,1)} + C_{-\pi/4, \pi/4}$ in ξ -coordinate. Dots: points $\xi_j = \chi_{\omega_1, \omega; b}(y_j) = i\omega_1 + b \sinh(i\omega + y_j)$ used in the simplified trapezoid rule. Dots-dashes: boundaries of the image $\chi_{\omega_1, \omega; b}(S_{(-d, d)})$ of the strip of analyticity $S_{(-d, d)}$. Upper panel: $\omega_1 = \omega = 0$, $d = \pi/4$, $b = 1/\sin(\pi/4)$. Lower panel: $\omega_1 = -1$, $\omega = d = \pi/8$, $b = 2/\sin(\pi/8)$. For the calculations represented in the lower panel, only a smaller domain $S_{(-1,1)} + C_{0, \pi/4}$ matters.

calibrated to the S&P implied volatility surface as of 7 January 2010 in⁴ [34, §5.2], and re-used in other studies, e.g. [25, 32, 63]. We see that Gauss-Legendre quadrature is less accurate than Gauss-Laguerre quadrature (for moderate numbers of nodes, at least), and the errors of Gauss-Laguerre quadrature are sufficient for reliable calibration, but only if the number of nodes N is chosen correctly. Note that a very large N cannot be chosen if double precision arithmetic is used, especially if very accurate evaluation of the integrand is difficult. The theoretical error bound in terms of the derivatives of the integrand, of high order, gives an infinite upper bound unless time to maturity is large. In order to obtain reliable calibration results, one has to resort to adaptive quadratures, and the CPU time inevitably increases. If an ad-hoc N is prefixed, calibration errors may result. See Fig. 2, where the curves calculated using Gauss-Laguerre quadrature wiggle for $N = 60, 100, 125$, but are only marginally different from the correct one for $N = 150$. We do not show the latter curve because it is only marginally different from the correct one; on the graph, the difference is seen in the far left tail only.

⁴The parameters in (1.3) can be found in the published version of [34], but not in the preprint.

TABLE 1. Benchmark prices V of OTM and ATM options of short maturity $T = 1/252$, spot $S_0 = 1$, in the rough Heston model with the parameters (1.3) and relative errors of SINH-CB, Gauss-Laguerre and Gauss-Legendre quadratures w.r.t. V . N is the number of terms.

K	0.95	0.975	1	1.025	1.05	N
V	2.4557955E-07 1.20E-07	1.29117047E-04 8.79E-10	5.0111443104E-03 7.42E-11	9.16277402E-05 7.27E-10	3.3118E-08 -8.94E-06	105
$SINH_1$	4.02E-06	9.19E-07	2.78E-08	-9.00E-07	-7.86E-06	70
$SINH_2$	3.70E-06	9.18E-07	2.78E-08	-9.01E-07	-1.03E-05	61
$Gauss - Laguerre$	-1.16E-03 -1.94E-04	-1.32E-06 5.38E-07	-3.05E-08 1.79E-08	-4.13E-06 -1.45E-06	-9.05E-03 -1.55E-03	125 150
$Gauss - Legendre$	-9.40E-01 9.60E-02	1.35E-04 8.99E-05	1.07E-07 -2.19E-08	3.19E-05 8.39E-06	3.70E+00 1.01E+00	150 200

Absolute errors of the benchmark prices are less than $E - 13$.

$SINH_1, SINH_2$: SINH-CB with $\omega = \pm 0.1, \omega = \pm 0.2$, respectively, is used to price the covered call.

For each ω , parameters ω_1 and b are chosen the universal recommendation for the strip of analyticity $S_{(-1,0)}$

$SINH_1$: ζ is chosen using the universal recommendation for error tolerance $E - 10$, $\Lambda = N\zeta$ is 20% larger than the general prescription recommends. $SINH_2$: ζ is 5% smaller, and Λ 10% larger than recommended.

In all cases, the BL Modification of Adams method is used with $M = 1000$; V is calculated using $M = 20000$.

Errors of the Gauss-Laguerre method with $N = 175$ is of the same order as the ones for $N = 150$

If the Gauss-Laguerre method is used with $N = 200$, the program written in Matlab (hence, double-precision arithmetic is used) produces NA

. Errors of the Gauss-Legendre method with $N = 225$ are larger than the ones for $N = 200$

If $M = 10000$ or $M = 20000$ is used, the errors remain essentially the same.

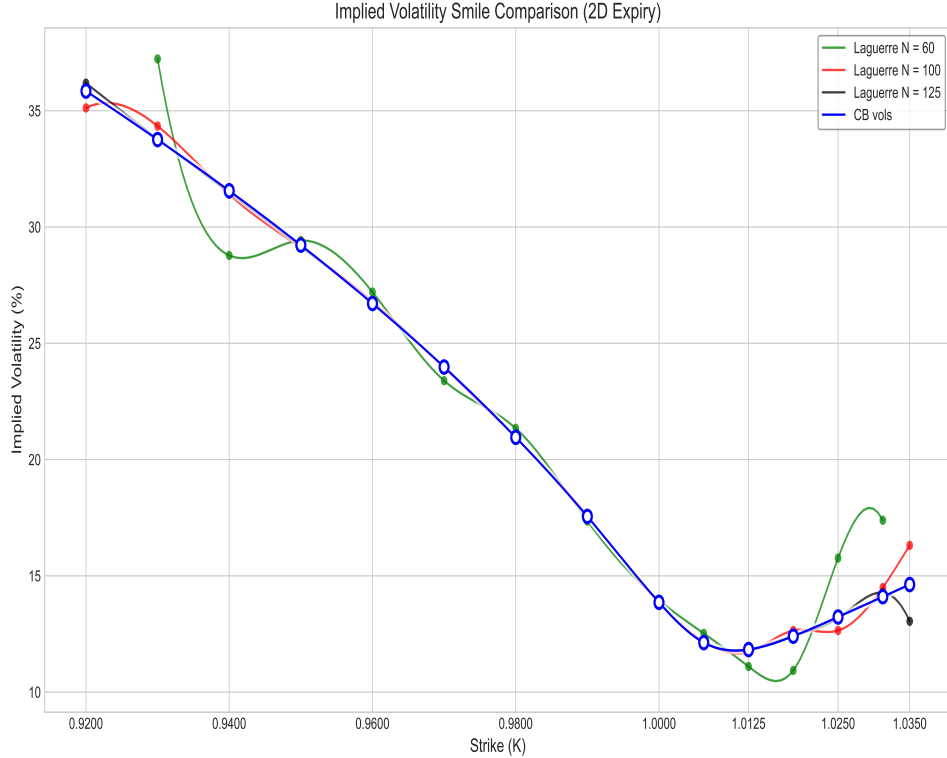


FIGURE 2. Implied volatility curves; the parameters are $(\alpha, \gamma, \theta, \nu, \rho, v_0) = (0.6, 2.0, 0.025, 0.2, -0.6, 0.025)$ as in Example 6.2 in [32].

The rest of the paper is organized as follows. In sect. 2, we recall basic formulas related to the rough Heston model and its Markovian approximation. The fractional Adams method, its modification and examples of the errors of the former are described in sect. 3. Sources of errors of several popular methods for the Fourier inversion are discussed and an explicit algorithm of the SINH-CB method is described in sect. 4; several tables with numerical examples and figures that illustrate errors of different methods are in sect. 5. In sect. 6 we outline a reliable and fast calibration procedure based on the Conformal Bootstrap principle and sinh-acceleration, and in sect. 7 produce calibration examples. The same schemes can be applied to any model where option prices are calculated using the inverse Fourier transform. In section 7.2 we show the calibration pitfalls that can result from using a seemingly accurate pricer with universal numerical settings. In sect. 8, we explain the importance of the SINH-CB method for risk-management and market-making, and summarize the results of the paper. A modification of the Adams method with non-uniform grids and additional Figures and Tables can be found in the Appendix.

2. ROUGH HESTON MODEL AND ITS MARKOVIAN APPROXIMATION

2.1. Formulas for the characteristic function. The rough Heston model [34] is constructed by replacing the variance process in the Heston model with the fractional square root process:

$$(2.1) \quad dS_t = S_t \sqrt{V_t} dB_t,$$

$$(2.2) \quad V_t = V_0 + \frac{1}{\Gamma(H+1/2)} \int_0^t (t-s)^{H-1/2} (\gamma(\theta - V_s) ds + \gamma\nu \sqrt{V_t} dW_s),$$

where $S_0, V_0 > 0$ and (B_t, W_t) is BM in 2D with the correlation coefficient $\rho \in [-1, 1]$; the components are standard BM in 1D. Denote $\alpha = H+1/2$, and let $\alpha \in (0, 1)$, $v, \gamma, \theta, \nu > 0$. It is proved in [34, 33] that the (conditional) characteristic function of the log-price $\Phi_\alpha(t, T, v, \xi) := \mathbb{E}[e^{i\xi X_T} \mid X_t = 0, V_t = v]$ in the rough Heston model is of the form

$$(2.3) \quad \Phi_\alpha(t, T; v, \xi) = \exp[g_1(\xi, \tau) + vg_2(\xi, \tau)],$$

where $\tau = T - t$,

$$(2.4) \quad g_1(\xi, \tau) = \theta\gamma \int_0^\tau h(\xi, s) ds, \quad g_2(\xi, \tau) = I^{1-\alpha} h(\xi, \tau),$$

and $h(\xi, \cdot)$ is the solution of the fractional Riccati equation

$$(2.5) \quad D_t^\alpha h(\xi, t) = -\frac{1}{2}(\xi^2 + i\xi) + \gamma(i\xi\rho\nu - 1)h(\xi, t) + \frac{(\gamma\nu)^2}{2}h(\xi, t)^2,$$

subject to $I^{1-\alpha} h(\xi, 0) = 0$. Recall that, for $\alpha \in (0, 1)$, I^α and D^α are the fractional integral and differential operators:

$$(2.6) \quad I^\alpha u(t) = \frac{1}{\Gamma(\alpha)} \int_0^t (t-s)^{\alpha-1} u(s) ds,$$

$$(2.7) \quad D^\alpha u(t) = \frac{1}{\Gamma(1-\alpha)} \frac{d}{dt} \int_0^t (t-s)^{-\alpha} u(s) ds.$$

Introduce the notation

$$(2.8) \quad F(\xi, h) = -\frac{1}{2}(\xi^2 + i\xi) + \gamma(i\xi\rho\nu - 1)h + \frac{(\gamma\nu)^2}{2}h^2.$$

Equation (2.5) subject to $I^{1-\alpha}h(\xi, 0) = 0$ is equivalent to the following Volterra equation

$$(2.9) \quad h(\xi, t) = I^\alpha F(\xi, t) = \frac{1}{\Gamma(\alpha)} \int_0^t (t-s)^{\alpha-1} F(\xi, h(\xi, s)) ds.$$

In [34], (2.9) is solved (numerically) using the fractional Adams method. It is not explained how g_1 and g_2 are evaluated. Presumably, using the piece-wise linear interpolation as in the fractional Adams method: the trapezoid rule and fractional trapezoid rule, respectively. Since h is not smooth at 0 and an additional fractional integral needs to be evaluated, the errors increase. We use the following version of (2.3), thereby avoiding additional errors.

Proposition 2.1. *Let $\alpha \in (0, 1)$, $v, \gamma, \theta, \nu > 0$, $\rho \in (-1, 1)$, and let $h(\xi, t)$ be the solution of (2.9). Then*

$$(2.10) \quad \Phi_\alpha(t, T, v, \xi) = \exp \left[\int_0^T (\gamma\theta h(\xi, s) + vF(\xi, h(\xi, s))) ds \right].$$

Proof. It suffices to note that $I^{1-\alpha}I^\alpha = I^1$. □

2.2. Asymptotics of $\phi(\xi, \tau) := g_1(\xi, \tau) + vg_2(\xi, \tau)$ as $\tau \rightarrow \infty$. The asymptotic formula is an analog of the formula rigorously derived in [51] in the Heston model. Unfortunately, we were unable to rigorously prove the formula in the case of the rough Heston model and the validity of the assumption that $\phi(\xi, \tau)$ admits analytic continuation to an open cone \mathcal{C} containing $(0, +\infty)$. We verified the latter property for a number of sets of the parameters of the model using the conformal bootstrap principle. The second assumption that we make is that as $\xi \rightarrow \infty$ remaining in \mathcal{C} ,

$$(2.11) \quad h(\xi, \tau) = h_\infty \xi + O(1),$$

where $h_\infty \in \mathbb{C} \setminus \{0\}$. We also empirically verified this assumption in a number of examples. Substituting (2.11) into (2.9), dividing by ξ and passing to the limit $\xi \rightarrow \infty$, we observe that (2.11) fails unless h_∞ is a solution of the equation

$$-\frac{1}{2} + i\rho\gamma\nu h_\infty + \frac{(\gamma\nu)^2}{2}h_\infty^2 = 0.$$

As in the case of the Heston model, we need the solution in the left half-plane, therefore,

$$(2.12) \quad h_\infty = -\frac{i\rho + \sqrt{1 - \rho^2}}{\gamma\nu}.$$

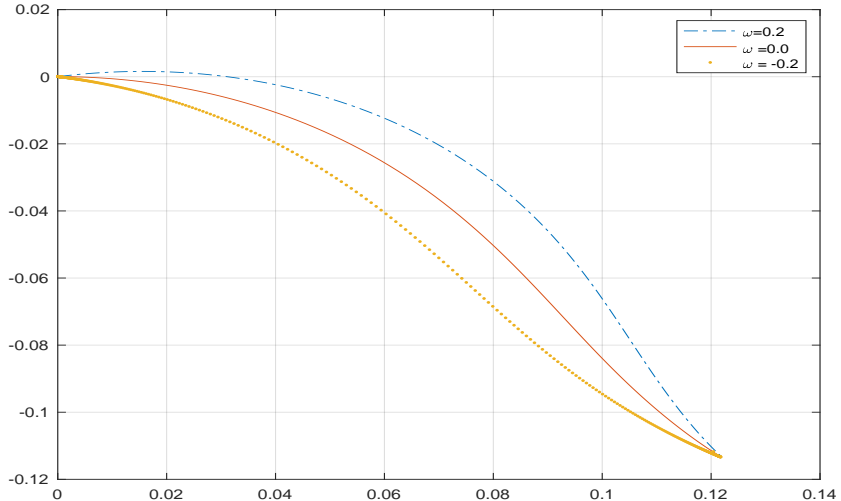
Now we can calculate the asymptotics of $\phi(\xi, \tau)$:

$$(2.13) \quad \phi(\xi, \tau)/\xi = \gamma\theta h_\infty \tau + \frac{v_0 h_\infty}{\Gamma(1-\alpha)} \int_0^\tau (\tau-s)^{-\alpha} ds + o(1) = -c_\infty(\tau) + o(1),$$

where

$$(2.14) \quad c_\infty(\tau) = (-h_\infty) \left(\gamma\theta\tau + \frac{v_0\tau^{1-\alpha}}{\Gamma(2-\alpha)} \right),$$

FIGURE 3. Curves $\mathcal{L}_{\omega_1, b, \omega} \ni \xi \mapsto -\phi(\xi, \tau)/\xi \in \mathbb{C}$ for $\omega = -0.2, 0.0, 0.2$ and $\tau = 1/252$. Parameters of the rough Heston model are in (1.3), $c_\infty(\tau) = 0.1222 - 0.1136i$. We observe a small discrepancy in the imaginary part of $c_\infty(\tau)$. For the choice of $\Lambda = N\zeta$, only the real part is used.



where in turn $v_0 := V_0$. Note that if $\alpha = 1$, then the asymptotic formula (2.13) coincides with the formula for the Heston model derived in [51]. We observed that numerically calculated ϕ satisfies $\phi(\xi, \tau)/\xi \rightarrow c_\infty(\tau)$ with a good accuracy. See Fig. 3.

2.3. A generalization of (2.10). In [47, Theorem 4.3 and Example 7.2] (see also [25, Eq. (9)-(10), (12)]), one finds a generalization of the rough Heston model [34]. Assuming $\text{Im } \xi \in [-1, 0]$ and $\text{Im } \eta \leq 0$, the characteristic function of the joint distribution of (X_T, V_T)

$$\Phi_\alpha(t, T, v, \xi, \eta) := \mathbb{E}[e^{i\xi X_T + i\eta V_T} \mid X_t = 0, v_T = v]$$

admits the representation

$$(2.15) \quad \Phi_\alpha(t, T, v, \xi, \eta) = \exp[g_1(\xi, \eta, \tau) + vg_2(\xi, \eta, \tau)],$$

where $\tau = T - t$, g_1 and g_2 are defined via a function $h(\xi, \eta, \tau)$ as above. For (ξ, η) fixed, $h(\xi, \eta, t)$ is the solution to the Volterra equation

$$(2.16) \quad h(\xi, \eta, t) = \frac{1}{\Gamma(\alpha)} \left(i\eta t^{\alpha-1} + \int_0^t (t-s)^{\alpha-1} F(\xi, h(\xi, \eta, s)) ds \right),$$

where $F(\xi, h)$ is given by (2.8). Applying $I^{1-\alpha}$ to (2.16) and taking into account that $I^{1-\alpha} t^{\alpha-1} = \Gamma(\alpha)$, we obtain the following analog of Proposition 2.1.

Proposition 2.2. *Let $\alpha \in (0, 1)$, $v, \gamma, \theta, \nu > 0$, $\rho \in (-1, 1)$, and let $h(\xi, \eta, t)$ be the solution of (2.16). Then*

$$\Phi_\alpha(t, T, v, \xi, \eta) = \exp \left[i\eta \left(v + \frac{\gamma\theta t^\alpha}{\Gamma(\alpha+1)} \right) + \int_0^\tau (\gamma\theta h(\xi, \eta, s) + v F(\xi, h(\xi, \eta, s))) ds \right].$$

Note that an accurate numerical solution of (2.16) requires different and more involved modifications of the Adams method than the ones in the present paper; we will consider (2.16) in a separate publication.

2.4. Markovian approximation of rough volatility. The rough Heston model is characterized by a fractional integral in the dynamics of the volatility process. The key idea of the Markovian approximation is to replace the non-Markovian fractional process with a high-dimensional Markovian process that has similar dynamics [7]. One observes that the fractional kernel of the rough Heston model $K(t) = c_\alpha t^{\alpha-1}$ is a complete monotone function, hence, by Bernstein's theorem, can be represented as an integral of exponential functions:

$$K(t) = \int_0^\infty e^{-yt} \mu(dy),$$

where $\mu(dy)$ is a positive measure. One approximates $\mu(dy)$ by a weighted sum of atoms, thereby approximating $K(t)$ by a finite weighted sum of exponentials:

$$(2.17) \quad K^n(t) = \sum_{j=1}^n c_j e^{-y_j t}.$$

The weights c_i and exponents y_i are chosen in order to match the original kernel $K(t)$ as closely as possible. This transforms the original non-Markovian rough Heston model into a higher-dimensional, but Markovian, system which is more amenable to standard pricing techniques. Following [7, §1], we can define the approximation (S^n, V^n) of (S, V) as follows

$$(2.18) \quad dS_t^n = S_t^n \sqrt{V_t^n} dB_t, \quad S_0^n = S_0,$$

$$(2.19) \quad V_t^n = V_0 + \int_0^t K^n(t-s) \gamma(\theta - V_s^n) ds + \int_0^t K^n(t-s) \gamma \nu \sqrt{V_s^n} dW_s.$$

In [46] it was shown that V^n solves an n -dimensional SDE. In [7], different schemes for the approximations K^n are compared, including those proposed in earlier studies, e.g. in [46], [2], [6]. Of these, the scheme called “BL2” was shown in [7] to be the fastest and most accurate. This rule minimizes the L^2 error between K^N and K , while penalizing large nodes. The corresponding algorithm can be found in Appendix F of [7].

The SINH-CB method can be applied in this setting to price not only European options, but barrier and lookback options as well, after the approximation by a regime-switching Lévy model or time discretization, and using the schemes in [22, 21, 20, 23].

3. FRACTIONAL ADAMS METHOD AND ITS MODIFICATION

3.1. Prediction-correction method (a.k.a. Adams method). One fixes a uniform grid $(t_j)_{j \in \mathbb{Z}_+}$, $t_j = j\Delta$, and calculates the approximations $\hat{h}(\xi, t_k)$, $k = 1, 2, \dots$, in two steps. First, the predictor $\hat{h}^P(\xi, t_k)$, $k = 1, 2, \dots$, is calculated, and then the more accurate approximation $\hat{h}(\xi, t_k)$, $k = 1, 2, \dots$. To calculate the former, the rectangular rule is used. At this step, in the region of large $|\xi|$ and small t_j , significant errors appear. The errors are especially clearly seen at the first step of the induction procedure, which we write explicitly:

$$(3.1) \quad \hat{h}^P(\xi, t_1) = b_{0,1} F(\xi, \hat{h}(\xi, t_0)) = b_{0,1} (-0.5(\xi^2 + i\xi)),$$

where $b_{0,1} = \Delta^\alpha / \Gamma(\alpha + 1)$. The RHS of (3.1) is of the order of $\Delta^\alpha |\xi|^2$, however,

$$(3.2) \quad \hat{h}(\xi, t) = -\frac{1}{2} \frac{(\xi^2 + i\xi)}{\Gamma(\alpha + 1)} t^\alpha (1 + o(1)),$$

uniformly in (ξ, t) in the region $\{(\xi, t) \mid 0 \leq t^\alpha |\xi|^2 < c\}$. See [25], where the full asymptotic expansion is calculated. We construct a modification of the Adams method changing the prediction step so that the asymptotics (3.2) is taken into account. We use the same coefficients $a_{j,k}$ as in the fractional Adams method. For $k = 0, 1, \dots, M-1$, set

$$a_{k+1,k+1} = \frac{\Delta^\alpha}{\Gamma(\alpha + 2)}, \quad a_{0,k+1} = \frac{\Delta^\alpha}{\Gamma(\alpha + 2)} (k^{\alpha+1} - (k - \alpha)(k + 1)^\alpha),$$

and, in a cycle $j = 1, 2, \dots, k$, calculate

$$a_{j,k+1} = \frac{\Delta^\alpha}{\Gamma(\alpha + 2)} ((k - j + 2)^{\alpha+1} + (k - j)^{\alpha+1} - 2(k - j + 1)^{\alpha+1}).$$

3.2. BL modification of Adams method. In the first version of the paper, it is the most efficient Modification III. Introduce the scaled unknown and its leading asymptotic part

$$\tilde{\hat{h}}(\xi, t) := (1 + |\xi|)^{-1} \hat{h}(\xi, t), \quad \tilde{\hat{h}}_{as}(\xi, t) := (1 + |\xi|)^{-1} \hat{h}_{as}(\xi, t),$$

where

$$\hat{h}_{as}(\xi, t) = -\frac{1}{2} \frac{(\xi^2 + i\xi)}{\Gamma(\alpha + 1)} t^\alpha.$$

Define the scaled remainder $\tilde{\hat{h}}^1(\xi, t) := \tilde{\hat{h}}(\xi, t) - \tilde{\hat{h}}_{as}(\xi, t)$, and use, in place of the function $F(\xi, h)$ given by (2.8), the transformed version

$$(3.3) \quad \tilde{F}_{as1}(\xi, \tilde{\hat{h}}_{as}, \tilde{\hat{h}}^1) = \gamma(i\xi\rho\nu - 1)(\tilde{\hat{h}}_{as} + \tilde{\hat{h}}^1) + (1 + |\xi|) \frac{(\gamma\nu)^2}{2} (\tilde{\hat{h}}_{as} + \tilde{\hat{h}}^1)^2.$$

Set $\tilde{\hat{h}}^1(\xi, 0) = 0$, and then, in a cycle $k = 0, 1, \dots, M-1$,

TABLE 2. Prices V of OTM and ATM options of maturity $T = 1/52$, spot $S_0 = 1$, in the rough Heston model with the parameters (1.3) calculated using the SINH-CB and Adams methods, and their relative errors (RE) w.r.t. prices calculated using SINH-CB method and BL Modification of the Adams method

K	0.8	0.85	0.9	0.95	1	1.05	1.1	1.15
V	1.78E-05	1.89042E-04	1.390943E-03	6.975898E-03	0.023896768	6.556374E-03	9.78149E-04	6.73E-05
RE	6.25E-05	5.39E-04	2.45E-03	-8.77E-01	-6.72E-07	-3.71E-02	-1.88E-01	-4.62E-01

1. Calculate $\tilde{h}_{as}(\xi, t_{k+1})$, then evaluate the predictor

$$(3.4) \quad \tilde{h}_0(\xi, t_{k+1}) = \sum_{0 \leq j \leq k} a_{j,k+1} \tilde{F}_{as1}(\xi, \tilde{h}_{as}(\xi, t_j), \tilde{h}^1(\xi, t_j)),$$

$$(3.5) \quad \tilde{h}^1(\xi, t_{k+1}) = \tilde{h}_0(\xi, t_{k+1}) + a_{k+1,k+1} \tilde{F}_{as1}(\xi, \tilde{h}_{as}(\xi, t_{k+1}), \tilde{h}^1(\xi, t_{k+1})).$$

2. For $m = 1, \dots, n$, perform the Picard correction

$$(3.6) \quad \tilde{h}^1(\xi, t_{k+1}) = \tilde{h}_0(\xi, t_{k+1}) + a_{k+1,k+1} \tilde{F}_{as1}(\xi, \tilde{h}_{as}(\xi, t_{k+1}), \tilde{h}^1(\xi, t_{k+1})).$$

3. Set the unscaled value

$$(3.7) \quad \hat{h}(\xi, t_{k+1}) := (1 + |\xi|) (\tilde{h}^1(\xi, t_{k+1}) + \tilde{h}_{as}(\xi, t_{k+1})).$$

4. Calculate the integral on the RHS of (2.10) using the trapezoid rule.

Remark 3.1. One can use asymptotic expansions of higher orders but in our numerical experiments with the two-term asymptotic expansion, the latter brings no advantages.

Remark 3.2. The differences between the results produced with our modification and those produced by the standard Adams method are sizable, and large for short maturities and large $|\xi|$. See Fig. 4. For options of moderate maturities, the real part of $\phi(t, T, v, \xi) := \ln \Phi_\alpha(t, T, v, \xi)$ in (2.10) decreases fast as the time to maturity $\tau := T - t$ increases. This explains why for options of moderate maturities, the error of the simplified trapezoid rule with several dozens of terms is smaller than E-06. In the case of $\phi(t, T, v, \xi, \eta) := \ln \Phi_\alpha(t, T, v, \xi, \eta)$ in (2.15), $\operatorname{Re} \phi(t, T, x, v, \xi, \eta)$ decreases if $\operatorname{Im} \eta \rightarrow +\infty$ as well, hence, evaluation of more complicated options using the Fourier inversion in 2D can be made fast as well: one needs to apply the sinh-acceleration w.r.t. η .

Remark 3.3. The accuracy of calculations can be increased using grids $\{t_k\}$ depending on ξ (see Sect. A.1). Non-uniform grids can be indispensable for pricing options of long maturities.

Remark 3.4. A pseudo-code implementation scheme for the BL Modification can be found in Appendix B.

Remark 3.5. BL-modification can be applied to more general kernels $K(t)$. Assume that (after the rescaling, if necessary) $K(t) = t^{\alpha-1}(1 + o(1))$ as $t \rightarrow 0+$. Then BL-modification is applied exactly as in the case $K(t) = t^{\alpha-1}$. Naturally, the coefficients of the Adams method must be recalculated for the given K . If more than one term of the asymptotics of $K(t)$ is available, additional asymptotic terms in BL-modification can be added. Additional terms can be added if $K(t) = t^{\alpha-1}$ as well but we found that adding one or two additional terms does

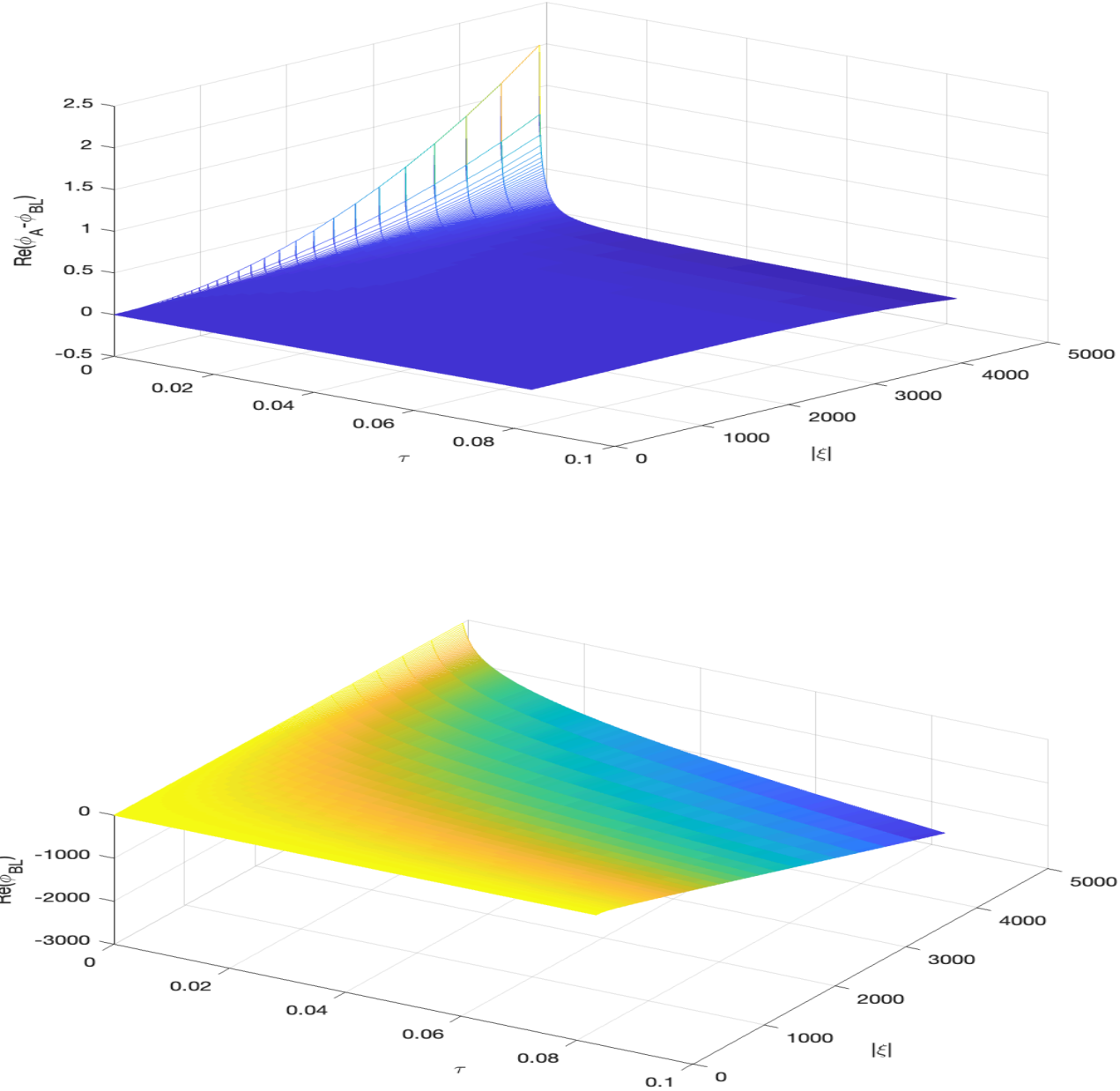


FIGURE 4. The rough Heston model with the parameters (1.3). Upper panel: difference between $\text{Re} \phi$ produced by the method [34] and $\text{Re} \phi$ using BL modification. In both cases, $T = 1/12$ and $M = 1000$. The nodes ξ are on the line $\{\text{Im} \xi = -0.5\}$. See Table 2. If $|\xi|$ are not small, it is seen that even at $T = 1/12$, the errors are not small, and for $T = 1/252$, the errors are large. Note that even marginally accurate evaluation of options of short maturity requires long grids. Lower panel: $\text{Re} \phi$ produced using BL modification

not improve the performance of BL-modification. If the kernel is regularized in the vicinity of 0, e.g., $K(t) := K(\epsilon, t) = (\epsilon + t)^{\alpha-1}(1 + o(t))$, where $\epsilon > 0$ is small parameter, then, in the formula for the leading term of $h(t)$, one replaces t^α with $(\epsilon + t)^\alpha$.

4. SEVERAL METHODS FOR FOURIER INVERSION

4.1. Flat iFT and simplified trapezoid rule. In popular models, the characteristic function admits analytic continuation to a strip around the real axis. This implies that the following scheme (standard from the viewpoint of Analysis) suggested in [12, 13, 14] is more efficient than the scheme in [43] based on the Lévy inversion formula. Let the riskless rate $r \geq 0$ be constant, and let $S_T = S_0 e^{X_T}$ be the price of the underlying non-dividend paying asset (or index) at time T . Let $\Phi(\xi, T) = \mathbb{E}[e^{i\xi X_T}]$ be the characteristic function of X_T under a no-arbitrage measure \mathbb{Q} chosen for pricing (the expectation is conditioned on the spot values of additional factors as in SV models). Then $\Phi(0, T) = 1$, and if $\mathbb{E}^{\mathbb{Q}}[e^{X_T}] < \infty$, $\Phi(-i, T) = e^{rT}$. Assume that there exist $\mu_-(T) < -1 < 0 < \mu_+(T)$ s.t. for $\beta \in (-\mu_+(T), -\mu_-(T))$, the exponential moments $\mathbb{E}^{\mathbb{Q}}[e^{\beta X_T}]$ are finite. Equivalently, $\Phi(\xi, T)$ admits analytic continuation to a strip $S_{(\mu_-(T), \mu_+(T))} := \{\xi \mid \text{Im } \xi \in (\mu_-(T), \mu_+(T))\}$. Then the price of the call option with strike K and maturity T can be calculated as follows. The payoff function $G(S_0, K, x) = (S_0 e^x - K)_+$ admits a representation

$$(4.1) \quad G(S_0, K; x) = \frac{1}{2\pi} \int_{\text{Im } \xi = \omega_1} e^{ix\xi} \hat{G}(S_0, K; \xi) d\xi,$$

where $\omega_1 \in (\mu_-(T), -1)$ is arbitrary, and $\hat{G}(S_0, K; \xi) = -K e^{i\xi \ln(S_0/K)} / (\xi(\xi + i))$ is the Fourier transform of $G(S_0, K; x)$ w.r.t. x . We substitute the integral representation (4.1) of $G(S_0, K; X_T)$ into the pricing formula $V(S_0, K; T) = e^{-rT} \mathbb{E}[(S_0 e^{X_T} - K)_+]$, and change the order of integration and summation (the use of the Fubini theorem can be justified in all popular models). The result is (1.1). Similarly, the price of the put is given by the RHS of (1.1) with arbitrary $\omega_1 \in (0, \mu_+(T))$ (repeat the proof for the call starting with $G(x) = (K - S_0 e^x)_+$ or use the put-call parity on the LHS of (1.1) and the residue theorem on the RHS). The price of the covered call is given by the RHS of (1.1) with $\omega_1 \in (-1, 0)$. Since $\overline{\Phi(\xi, T)} = \Phi(-\bar{\xi}, T)$ and $\overline{\hat{G}(\xi)} = \hat{G}(-\bar{\xi})$, an equivalent form of (1.1) is

$$(4.2) \quad V(S_0, K; T) = -\frac{K e^{-rT}}{\pi} \text{Re} \int_{\text{Im } \xi = \omega_1} \frac{e^{i\xi \ln(S_0/K)} \Phi(\xi, T)}{\xi(\xi + i)} d\xi.$$

After truncation, the integral on the RHS of (1.1) (or (4.2)) can be calculated using either trapezoid rule or Simpson rule.

However, since the integrand on the RHS of (1.1) is analytic in a strip $S_{(\lambda_-, \lambda_+)}$ around the line of integration ($\lambda_- = \mu_-(T)$, $\lambda_+ = -1$ in the case of calls, $\lambda_- = -1$, $\lambda_+ = 0$ in the case of the covered call, and $\lambda_- = 0$, $\lambda_+ = \mu_+(T)$ in the case of puts), it is significantly more efficient to use the infinite trapezoid rule and then truncate the sum. The reason is an exponential decay of the discretization error of the infinite trapezoid rule as the function of ζ , where ζ is the step. In Mathematical Finance, Lee [50] and Feng and Linetsky [36] were the first to use this important property of the infinite trapezoid rule; the truncation of the sum results in the simplified trapezoid rule. As it is stated in the review paper [62], the excellent properties of the simplified trapezoid rule had been noticed since Poisson but rigorously proved in the middle

of the last century only. Let $H^1(S_{(\lambda_-, \lambda_+)})$ denote the space of functions analytic in the strip $S_{(\lambda_-, \lambda_+)}$ such that

$$\int_{\lambda_-}^{\lambda_+} |f(\eta + i\omega)| d\omega \rightarrow 0 \quad \text{as } (\mathbb{R} \ni) \eta \rightarrow \pm\infty$$

and the following analog of the Hardy norm is finite:

$$(4.3) \quad \|f\|_{S_{(\lambda_-, \lambda_+)}} := \lim_{\omega \uparrow \lambda_+} \int_{\mathbb{R}} |f(\eta + i\omega)| d\eta + \lim_{\omega \downarrow \lambda_-} \int_{\mathbb{R}} |f(\eta + i\omega)| d\eta < \infty.$$

Fix $\omega_1 \in (\lambda_-, \lambda_+)$, and denote $d(\omega_1) = \min\{\omega_1 - \lambda_-, \lambda_+ - \omega_1\}$. For $\zeta > 0$, construct a grid $\xi = i\omega_1 + \zeta\mathbb{Z}$, and denote by $E_{\text{disc}}(\zeta, \infty)$ the error of the infinite trapezoid rule

$$\int_{\text{Im } \xi = \omega} f(\xi) d\xi \approx \zeta \sum_{j \in \mathbb{Z}} f(\xi_j).$$

The following bound is proved in [61] using the heavy machinery of the sinc-functions (a simple proof can be found in [51], and several other elementary bounds and proofs in [62]):

$$(4.4) \quad |E_{\text{disc}}(\zeta, \infty)| \leq \frac{e^{-2\pi d(\omega_1)/\zeta}}{1 - e^{-2\pi d(\omega_1)/\zeta}} \|f\|_{S_{(\lambda_-, \lambda_+)}}.$$

Let the error tolerance $\epsilon > 0$ for the discretization error be small, and let $|\mu_{\pm}|$ be not too large. Then we choose $\omega_1 = (\lambda_- + \lambda_+)/2$, set $d(\omega_1) = k_d(\lambda_+ - \lambda_-)/2$, where $k_d < 1$ is close to 1, e.g., $k_d = 0.95$, and use the following approximate recommendation:

$$(4.5) \quad \zeta = 2d(\omega_1) / \ln(100/\epsilon).$$

If the strip of analyticity is very wide, we choose a substrip around the line of integration with moderately large $|\lambda_{\pm}|$ and apply the prescription above.

Once ζ is chosen and the sum is truncated, we have the pricing formula. In the case of (1.1),

$$(4.6) \quad V(S_0, K; T) = -\frac{Ke^{-rT}\zeta}{2\pi} \sum_{|j| \leq N} \frac{e^{i\xi_j \ln(S_0/K)} \Phi(\xi_j, T)}{\xi_j(\xi_j + i)},$$

where $\xi_j = i\omega_1 + j\zeta$. The number of terms can be decreased almost two-fold: similarly to (4.2),

$$(4.7) \quad V(S_0, K; T) = -\frac{Ke^{-rT}\zeta}{\pi} \operatorname{Re} \sum_{0 \leq j \leq N} (1 - \delta_{j0}/2) \frac{e^{i\xi_j \ln(S_0/K)} \Phi(\xi_j, T)}{\xi_j(\xi_j + i)},$$

where δ_{jk} is the Kronecker symbol. We call this method Flat iFT (flat inverse Fourier transform) method. To choose N so that the truncation error is sufficiently small, it is necessary to know the rate of decay of $\Phi(\xi, T)$ as $\xi \rightarrow \infty$ along the contour of integration. Let $\Phi(\xi, T) = \exp[\phi(\xi, T)]$, and let an upper bound for $\operatorname{Re} \phi(\xi, T)$ be known:

$$(4.8) \quad \operatorname{Re} \phi(\xi, T) < -g(|\xi|, T),$$

where $g(|\xi|, T)$ is a monotonically increasing function of $|\xi|$. Then the truncation of the series at $|\xi| = \Lambda_0$ introduces the error of the order of $e^{-g(\Lambda_0, T)}/\Lambda_0$. If an analytic formula for $\phi(\xi, T) = \ln \Phi(\xi, T)$ is available, then an efficient bound (4.8) can be derived. See [51, 52]. In the case of the rough Heston model, an analytic formula is not available. In Sect. 4.9, we use an informally proved asymptotic formula (see Sect. 2.2) to formulate a prescription for the

choice of Λ_0 . In the case of Flat iFT, the asymptotic formula and the prescription should be used with $\omega = 0$. After Λ_0 is calculated, we set $N = \text{ceil } \Lambda_0/\zeta$.

The implementation of Flat iFT is very simple, and can be easily parallelized if the option prices for several dozens, hundreds of strikes or even thousands of pairs (K, T) need to be calculated. Furthermore, if the strip of analyticity is not too narrow and the characteristic function decays not too slowly, which is the case for the Heston model and options of not very short maturity, then N of the order of 2-3 hundreds suffices to satisfy the error tolerance of the order of E-07 (assuming that the strike $S_0 = 1$).

4.2. Carr-Madan method. Nevertheless, in noughties, the unnecessary complicated (and slower and less accurate) CM method became popular, and it is still used in the quantitative finance literature as *one of the standard methods*. Hence, the accurate analysis of the drawbacks of the CM method seems to be useful. The main idea of the method is to use the Fast Fourier transform (FFT) to evaluate the option prices at several strikes. However, FFT produces the results at points of uniformly spaced grids in the $\ln(K)$ -space. Therefore, in order to evaluate the option prices for given strikes, an interpolation procedure needs to be employed. To satisfy even a moderate error tolerance, a fine grid $x_j = x_0 + j\Delta$, $j = 1, 2, \dots, M = 2^m$, with $\Delta \ll 1$ is necessary; to make an accurate Fourier inversion, a small step ζ in the dual space must be used (in [26], $\zeta = 0.25$ or $\zeta = 0.125$ are recommended). The Nyquist relation $\Delta\zeta = 2\pi/M$ requires M to be of the order of several thousand. In [26], the basic recommendation is $M = 4,096$ and it is mentioned that larger $M = 8,192$ or $M = 16,384$ may be needed. Hence, the calculations become computationally many times costlier as compared to Flat iFT, and an unnecessary interpolation error is introduced. Table 10 illustrates the adverse impact of the interpolation errors on the quality of calibration: the number of strikes for which the calculated prices are outside the no-arbitrage bounds increases because of the interpolation. In the case of the rough Heston model, accurate evaluation of $\Phi(\xi, T)$ for ξ large in absolute value is especially difficult and time consuming. The implied volatility surface produced by CM method can significantly differ from the correct one (see Fig. 10). In particular, essentially flat volatility curves can become nice volatility smiles, and changing the dampening factor (the line of integration) in the CM method, while keeping the same step size and the grid size recommended in the CM method one can significantly change the smiles and surface. The implied volatility surface can significantly change as one changes the step and/or grid size. Furthermore, the errors are systematic, and, in many cases, prices of deep OTM options produced by CM method are “prices” of the systematic errors of the method, which can be “useful” to produce the implied volatility curves and surfaces one wants to produce.

4.3. Gaussian quadratures. The specific choice $\omega_1 = -1/2$ was suggested by A. Lewis and A. Lipton [54, 55], and the formula for the covered call was rewritten in the form

$$(4.9) \quad V(S_0, K; T) = -\frac{(K/S_0)^{1/2}}{\pi} \text{Re} \int_0^{+\infty} \frac{e^{iy \ln(S_0/K)} \Phi(T, -i/2 + y)}{y^2 + 0.25} dy.$$

In the Lewis method [53], it is recommended to change the variable in order to reduce to the integral over $(0, 1)$, and then apply the Gauss-Legendre quadrature. Numerical examples (see, e.g., Table 1) show that, in applications to the Heston model and rough Heston model, for the same number of nodes, the errors of the Gauss-Legendre quadrature are larger than the errors of the Gauss-Laguerre quadrature. Finally, note that the performance of the Lewis method

strongly depends on the choice of the change of variables. In our numerical experiments, the errors of Gauss-Legendre quadrature increased greatly when we used $y = -\ln u$ instead of $y = u/(1 - u)$. We also observe that 1) given the error tolerance, the SINH-CB method requires the number of nodes 2-5 times smaller than the Gauss-Laguerre quadrature; 2) Gauss-Kronrod method is significantly slower even for the built-in error tolerance, and, typically, produces errors larger than E-8 whereas SINH-CB satisfies this error tolerance with 20-40 terms, depending on the maturity.

We finish the discussion about the performance of Gaussian quadratures with the following general observations. If the integrand is sufficiently regular, then the convergence of Gaussian quadratures are the best ones. However, the general error bounds are in terms of derivatives of high order, hence, sizable errors are possible. The error of a Gaussian quadrature for analytic functions can be expressed as a contour integral in the complex plane. This representation allows for the analysis of the error in terms of the behavior of the integrand in the complex domain. The decay of the error is then related to the distance of the contour from the interval of integration and the analytic properties of the integrand. For instance, a review paper [30] starts with “Let Γ be a simple closed curve in the complex plane encompassing the interval $[-1, 1]$ and let \mathcal{D} be its interior. Suppose f is a function that is analytic in \mathcal{D} and continuous on \mathcal{D} .” However, after the reduction to a finite interval as the Lewis method recommends, the derivatives become highly irregular and, apparently, very large. At the same time, the integrand does not admit analytic continuation to a domain containing $[0, 1]$, hence, there is no theoretical reason to expect that the Gauss-Legendre and Gauss-Kronrod quadratures should perform well. In the examples that we consider both perform moderately well although the latter is too slow and the former insufficiently accurate close to maturity and far in the tails. In the same examples, the Gauss-Laguerre quadrature performs much better although the number of terms needed to satisfy moderately small tolerance is 2-5 times larger than the number of terms that SINH-CB method required; even Flat iFT-BM method required smaller number of terms. However, the situation with the Gauss-Laguerre quadrature is rather peculiar. The theoretical error bound gives infinity when applied to the same examples; for pricing in the Heston model with small volatility of variance and far from maturity, in the NIG model far from maturity and the KoBoL model of the order $\nu > 1$, the same theoretical bound guarantees the excellent convergence. In more detail, for the integral

$$(4.10) \quad I(f_0) = \int_0^{+\infty} f_0(y) dy,$$

the error admits a representation in terms of the function $f(y) := e^y f_0(y)$:

$$(4.11) \quad Err_{GL}(I(f_0); n) = \frac{n!}{2(2n)!} f^{(2n)}(y).$$

for some $y > 0$ (see [1, 25.4.45]). Hence, the general error bound is

$$(4.12) \quad |Err_{GL}(I(f_0); n)| \leq \frac{n!}{2(2n)!} \sup_{y>0} |f^{(2n)}(y)|,$$

therefore, the bound (4.12) is applicable only if $f^{(2n)}$ is uniformly bounded. Furthermore, the very proof of the convergence of the quadrature is valid in this case only. In the case of the

TABLE 3. Evaluation of $\int_0^\infty e^{-ay} dy$. Relative errors of the Gauss-Laguerre quadrature with N terms.

a	0.001	0.005	0.01	0.02
$N = 100$	-0.6798	-0.1440	-0.0207	-0.00043
$N = 125$	-0.6149	-0.0878	-0.0077	-5.88E-05
$N = 150$	-0.5569	-0.0535	-0.0029	-8.10E-06
$N = 175$	-0.5044	-0.0326	-0.0011	-1.11E-06

Heston model with the following SDE for the variance process,

$$(4.13) \quad dV_t = \kappa(m - V_t)dt + \sigma_0 \sqrt{V_t} dW_t, \quad V_0 = v_0,$$

the logarithm of Φ on the RHS of (4.9) obeys the asymptotics

$$(4.14) \quad \operatorname{Re} \Phi(T, -i/2 + y) = -\frac{(\kappa m T + v_0) \sqrt{1 - \rho^2}}{\sigma_0} y (1 + O(y^{-1})).$$

Therefore, if $a := \frac{(\kappa m T + v_0) \sqrt{1 - \rho^2}}{\sigma_0} < 1$, there is no reason to expect that the Gauss-Laguerre quadrature should work, as it seen from Table 3, where we show the errors of the Gauss-Laguerre quadrature applied to $f_0(y) = e^{-ay}$ for various a and various number of terms. However, if $a \geq 1$, and $f(y) = e^y f_0(y)$ admits analytic continuation to a strip $S_{(-d,d)}$ around the real axis, and it is uniformly bounded in the strip, then, applying the Cauchy theorem, one easily proves that there exists $H > 0$ such that $\sup_{y>0} |f^{2n}(y)| \leq H d^{2n}$, and the bound (4.11) can be simplified

$$(4.15) \quad |\operatorname{Err}_{GL}(I(f_0); n)| \leq H \frac{n!}{2(2n)!} d^{2n}.$$

Hence, the rate of convergence of the quadrature is excellent.

Miraculously, if $a < 1$ is not very small, the errors are small; but for very small a , the errors become really huge. The rate of decay of the characteristic function very close to maturity is very small, and this is the region where the differences in the performance of different models are most clearly seen. Hence, the comparative results of the performance of different models using the Gauss-Laguerre quadrature are unreliable.⁵

In a market regime characterised by small v_0 and large σ_0 , e.g. on a post-earnings day in a calm bull market, the Gauss-Laguerre approach to Fourier inversion for Heston, and especially rough Heston, can become numerically fragile, especially at short expiries and for far-OTM strikes. The combination of very small initial variance and large volatility of variance causes the characteristic function to oscillate rapidly and decay slowly along the integration contour, especially for short maturities, where the effective spectral parameter is large, and if the sinh contour deformation is not used. In addition, since without the sinh deformation the integrand is highly oscillatory and only weakly damped, the fractional Adams method will typically require many more steps for the same level of accuracy. Since the Adams method is the main numerical bottleneck in the rough Heston price calculation, this will typically result in longer

⁵For KoBoL processes (a.k.a CGMY model) of order $\nu < 1$ and Variance Gamma model, the performance of the Gauss-Laguerre quadrature is much worse; for KoBoL processes of order $\nu > 1$, the performance is excellent. See Tables 15 and 16.

computation times. Even in the example of the calibration to TSLA implied vols, described in section 7, where v_0 is not small, one needs at least $N = 125$ Gauss-Laguerre nodes and $M = 500$ in order to obtain a relative error lower than 0.1% at 2D expiry ($T = 2/365$), for prices higher than 10^{-4} , whereas SINH needs on average $N = 67$ and $M = 180$, respectively.

4.4. COS method [35]. Both the pricing density and payoff are truncated and approximated by linear combinations of cosines. Thus, two unnecessary truncation errors are introduced. The error control becomes very difficult: the numerical scheme is characterized by 3 parameters. The truncation errors are controlled by the choice of two parameters, and, assuming that these are chosen sufficiently accurately, the geometric convergence of the method is illustrated by increasing the third parameter, the number of terms. The recommendations (in the literature, one can find several versions) are formulated in terms of the first 4 or 6 moments of the cumulant. In view of the exponential growth of the payoff of the call, any recommendation for the choice of the truncation parameters in terms of the moments cannot be reliable, and the authors of the COS method explicitly and strongly recommend to apply the method to price puts but not calls (see Remark 5.2 in [35]). As numerical examples in [15, 16] demonstrate, typically, given the error tolerance, Flat iFT requires a smaller number of terms than COS; in addition, Flat iFT is free from the unnecessary errors and restrictions of COS.

4.5. SINC method. The SINC method [5] is a modification of COS, with a more accurate approximation of the integrand after the truncation. The authors claim that 1) the new truncation recommendation is more efficient than the one in the COS method; 2) the truncation being made, approximation using sinc-functions is superior to the approximation used in the COS method. They also state that the number of terms required by the SINC method is 4 times smaller, at best, and, in some cases, COS is more accurate for the same number of terms. The theoretical error bounds in [5] are rather complicated, not explicit and essentially impossible to apply in practice. The numerical example in [5, Table 2] (pricing put in the Heston model) demonstrates the resulting errors. Naturally, to hide the errors, [5, Table 2] shows relative errors of put options in both OTM and ITM regions, the errors for ITM puts being excellent. However, when we use the numbers shown in [5, Table 2] to calculate the relative errors of the corresponding OTM calls, the errors become quite substantial. See Table 4. Next, the excellent performance of the infinite trapezoid rule is also explained in [61] using the approximation by linear combinations of SINC functions. In the result, the method in [5] uses approximately the same number of terms or even larger than even Flat iFT, to say nothing of the Flat iFT-BM and SINH-CB methods constructed below. Finally, note that in the example shown in [5, Table 2], the strip of analyticity of $\Phi(\xi, T)$ is very wide, as in the example for the KoBoL (a.k.a. CGMY) model in the same paper. In COS, SINC and Flat iFT methods, the number of terms is approximately inversely proportional to the width of the strip of analyticity. If the strip were narrow (as it is the case for the Heston model for T close to the moment explosion), both COS and SINC methods would have required several times more terms; very close to the explosion, thousands times more. The SINH-CB method is much less sensitive to the width of the strip of analyticity and requires small or moderate numbers of terms in all cases.

4.6. Flat iFT-BM and Flat iFT-NIG methods. The additional errors of COS are partially compensated by the increase of the width of the strip of analyticity around the line of integration: instead of one of the three strips $S_{(\mu_-(T), -1)}, S_{(-1, 0)}, S_{(0, \mu_+(T))}$, the strip $S_{(\mu_-(T), \mu_+(T))}$

can be used. In this section, we demonstrate that the same effect is achievable without introducing additional errors. We use the same straightforward idea as in [18], where we eliminated the zero at $\xi = 0$ of the integrand in the formula for the cumulative probability distribution function of a stable Lévy process. In the current setting, we eliminate two zeros, at $\xi = 0$ and $\xi = -i$. Let $\Phi_{ad}(\xi, T)$ be the characteristic function in a model, where vanilla prices can be calculated faster than in the initial model. Denote by $V_{call}(\Phi; S_0, K; T)$ the call price in the model with the characteristic function Φ ; as above, the asset pays no dividends and interest rate r is constant.

Proposition 4.1. *Let $\Phi(\xi, T)$ and $\Phi_{ad}(\xi, T)$ admit analytic continuation to a strip $S_{(\mu_-(T), \mu_+(T))}$, where $\mu_-(T) < -1 < 0 < \mu_+(T)$, and let $\Phi(-i, T) = \Phi_{ad}(-i, T) = e^{rT}$.*

Then, for any $\omega_1 \in (\mu_-(T), \mu_+(T))$,

$$(4.16) \quad V_{call}(\Phi; S_0, K; T) = V_{call}(\Phi_{ad}; S_0, K; T) - \frac{Ke^{-rT}}{2\pi} \int_{\text{Im } \xi = \omega_1} \frac{e^{i\xi \ln(S_0/K)} (\Phi(\xi, T) - \Phi_{ad}(\xi, T))}{\xi(\xi + i)} d\xi.$$

The equality (4.16) is valid for put and covered calls as well.

Proof. Let $\omega_1 \in (\mu_-(T), -1)$. Then (4.16) is valid. The apparent singularities of the integrand are removable because $\Phi(\xi, T) - \Phi_{ad}(\xi, T)$ is analytic in the strip $S_{(\mu_-(T), \mu_+(T))}$ and $\Phi(\xi, T) - \Phi_{ad}(\xi, T) = 0$ at $\xi = 0, -i$. Hence, the integrand on the RHS of (4.16) is analytic in the strip, and one may move the line of integration to any line $\{\xi \mid \text{Im } \xi = \omega_1\}$, $\omega_1 \in (\mu_-(T), \mu_+(T))$. The proof for puts and covered calls is essentially the same. \square

The integral on the RHS of (4.16) is calculated using Flat iFT. If $\mu_+(T) - \mu_-(T) \gg 1$, and $\omega_1(T) = (\mu_+(T) + \mu_-(T))/2$ is chosen, the half-width of the strip of analyticity used to derive the recommendation for the choice of the step ζ and ζ increase significantly, and the number of terms of the simplified trapezoid rule and CPU time decrease, also significantly.

Natural choices for Φ_{ad} are the characteristic functions in the following models:

- (1) the BM with the characteristic exponent $\psi(\xi) = \sigma^2 \xi^2/2 - i\mu\xi$; $\sigma > 0$, $\mu = r - \sigma^2/2$;
- (2) Normal Inverse Gaussian process (NIG) [3] or the generalization of NIG (tempered stable Lévy processes (NTS) constructed in [4]), with the same or wider strip of analyticity;
- (3) in applications to rough Heston model, it is feasible that the use of Φ_{ad} in the Heston model with the same parameters $\gamma, \theta, \nu, \rho$ can be advantageous.

We call the resulting method with the choices (1) and (2) *Flat iFT-BM* and *Flat iFT-NIG* (more generally, *Flat iFT-NTS*) methods. In the numerical examples in the paper, we use the simplest variant: Flat iFT-BM. In our numerical examples that we considered, the analogs: the Legendre-BM, Laguerre-BM and SINH-BM methods do not bring advantages as compared with the Lewis, Gauss-Laguerre and SINH-methods. We leave to the future the study of possible advantages of choices (2) and (3).

4.7. Summation by parts in the infinite trapezoid rule. For the explicit formulas, see [19]. The summation by parts significantly decreases the product ζN necessary to satisfy the given error tolerance if the strike is not close to the spot. Hence, it is natural to separate the region of strikes into two regions: close to the spot, where Flat iFT-BM (or Flat iFT-NIG) is used, and the region farther from the spot, where, in addition, the summation by parts is used.

4.8. SINH-acceleration. In the real-analytic interpretation [26], choices of different lines of integration are choices of different *dampening factors*. In Complex Analysis, one observes that the Fourier transform \hat{f} of a sufficiently regular function f is an analytic function in a wide region \mathcal{U}_0 of the complex plane and meromorphic function in a wider region \mathcal{U} . We choose \mathcal{U} so that $\hat{f}(\xi) \rightarrow 0$ sufficiently fast as $\xi \rightarrow \infty$ remaining in \mathcal{U} . The inverse Fourier transform can be calculated deforming the line of integration into any sufficiently regular curve in \mathcal{U}_0 ; crossing poles, one can reduce to the integral over any sufficiently regular curve in \mathcal{U} (plus residues at the poles crossed in the process of deformation). In the case of the Heston model, under additional restriction on the parameters, it is proved in [56] that $\Phi(T, \xi)$ is analytic in $\mathcal{U} = \mathbb{C} \setminus i((-\infty, \mu_-(T)] \cup [\mu_+(T), +\infty))$, where $\mu_-(T) < -1 < 0 < \mu_+(T)$; in [51], this fact is proved for jump-diffusion generalizations of the Heston model, with more than one factor driving the dynamics of the volatility process, and algebraic equations for $\mu_-(T)$ and $\mu_+(T)$ were derived. For wide classes of affine jump-diffusion processes, it is proved in [52] that $\Phi(\xi, T)$ is an analytic function on the union $\mathcal{U}_0(\mu_-(T), \mu_+(T), \gamma_-, \gamma_+)$ of a strip $S_{(\mu_-(T), \mu_+(T))}$, where $\mu_-(T) < -1 < 0 < \mu_+(T)$, and a cone $\mathcal{C}_{\gamma_-, \gamma_+} := \{\xi = \rho e^{i\varphi} \mid \varphi \in (\gamma_-, \gamma_+) \vee \varphi \in (\pi - \gamma_-, \pi - \gamma_+)\}$, where $\gamma_- \in (-\pi/2, 0), \gamma_+ \in (0, \pi/2)$ (typically, $\gamma_{\pm} = \pm\pi/4$, however, in the case of the Heston model, $\gamma_{\pm} = \pm\pi/2$), and decays as $\xi \rightarrow \infty$ remaining in the cone. Once the existence of such a strip and cone is established, we choose a deformation of the contour of integration into a contour $\mathcal{L}_{\omega_1, b, \omega} := \chi_{\omega_1, b, \omega}(\mathbb{R})$, where $\omega_1 \in \mathbb{R}, b > 0, \omega \in (\gamma_-, \gamma_+)$, and the conformal map $\chi_{\omega_1, b, \omega}$ (*sinh-deformation*) is defined by (1.2). The parameters of the deformation are chosen so that in the process of deformation, the contour remains in the domain of analyticity of $\Phi(\xi, T)$, and the singularities at 0 and $-i$ are not crossed. The deformation being made, we change the variable $\xi = \xi(y) = \chi_{\omega_1, b, \omega}(y)$ in (1.1)

$$(4.17) \quad V(S_0, K; T) = -\frac{bKe^{-rT}}{2\pi} \int_{\mathbb{R}} \frac{e^{i\xi(y) \ln(S_0/K)} \Phi(\xi(y), T)}{\xi(y)(\xi(y) + i)} \cosh(i\omega + y) dy,$$

and apply the simplified trapezoid rule:

$$(4.18) \quad V(S_0, K; T) = -\frac{b\zeta K e^{-rT}}{\pi} \operatorname{Re} \sum_{j=0}^N e^{i\xi(j\zeta) \ln(S_0/K)} g(j\zeta, T) (1 - \delta_{0j}/2),$$

where $g(y, T) = \frac{\Phi(\xi(y), T)}{\xi(y)(\xi(y) + i)} \cosh(i\omega + y)$. Explicit recommendations for the choice of the parameters of the deformation ω_1, b, ω and parameters ζ, N of the simplified trapezoid rule are derived in [17]. We add several useful details.

- I. Find $\mu_{\pm}(T)$ and γ_{\pm} .
- II. Calculate z_T using (4.19). If $z_T \leq 0$, use $\omega \leq 0$ and calculate the price of either the call or covered call; otherwise, use $\omega \geq 0$ and calculate the price of either the put or covered call.
- III. (a) If the call is priced, set $\lambda_- = \mu_-(T), \lambda_+ = -1, \omega = \gamma_-/2, d_0 = -\omega$.
(b) If the put is priced, set $\lambda_- = 0, \lambda_+ = \mu_+(T), \omega = \gamma_+/2, d_0 = \omega$.
(c) If the covered call is priced, set $\lambda_- = -1, \lambda_+ = 0$. If $S_0 < K$, set $\omega = \gamma_-(T)/2, d_0 = -\omega$. If $S_0 > K$, set $\omega = \gamma_+(T)/2, d_0 = \omega$.
(d) For ATM options, it is optimal to set $\omega = (\gamma_- + \gamma_+)/2, d_0 = (\gamma_+ - \gamma_-)/2$.

IV. Choose $k_d < 1$ close to 1, e.g., $k_d = 0.9$, and set $d = k_d d_0$, $\zeta = 2\pi d / \ln(100/\epsilon)$,

$$b = \frac{\lambda_+ - \lambda_-}{\sin(\omega + d) - \sin(\omega - d)}, \quad \omega_1 = \frac{\lambda_- \sin(\omega + d) - \lambda_+ \sin(\omega - d)}{\sin(\omega + d) - \sin(\omega - d)}.$$

V. As in the case of Flat iFT, to choose N so that the truncation error is sufficiently small, it is necessary to know the rate of decay of $\Phi(\xi, T)$ as $\xi \rightarrow \infty$ along the contour of integration. Let $\Phi(\xi, T) = \exp[\phi(\xi, T)]$, and let an upper bound (4.8) for $\operatorname{Re} \phi(\xi, T)$ be known. In the y -coordinate, the series decays as $(K\zeta b/\pi) e^{-g(|\xi(y_j)|, T)} / |\xi(y_j)|$. Since $|\xi(y)|$ increases as an exponential function of y as $y \rightarrow \pm\infty$, the truncation error is smaller than the last term of the truncated sum if $g(|\xi(y_j)|, T)$ is large. We find the positive solution Λ_0 of the equation $e^{-g(\Lambda_0, T)} / \Lambda_0 = b\pi\epsilon / (K\zeta)$, and set $\Lambda = \ln(2\Lambda_0 / (Kb))$, $N = \operatorname{ceil} \Lambda / \zeta$.

Remark 4.1. The recommendation $\zeta = 2\pi d / \ln(100/\epsilon)$ presumes that $\|f\|_{S_{(\lambda_-, \lambda_+)}}$, the analogue (4.3) of the Hardy norm of the integrand, is bounded by 100. A safer alternative which we used in several publications is to use the approximation $\|f\|_{S_{(\lambda_-, \lambda_+)}} \approx |f(i(\omega + d))| + |f(i(\omega - d))|$.

4.9. Ad-hoc bound for ϕ and choice of N in the rough Heston model. To choose $\Lambda := N\zeta$, we use (2.13)-(2.14). The leading term of asymptotics of the expression under the exponential sign in the pricing formula is

$$(-c_\infty(T) + i \ln(S_0/K))\xi = iz_T\xi - \operatorname{Re} c_\infty\xi,$$

where

$$(4.19) \quad z_T = \ln(S_0/K) - \frac{\theta\rho}{\nu}T - \frac{v_0\rho}{\Gamma(2-\alpha)}T^{1-\alpha},$$

$$(4.20) \quad \operatorname{Re} c_\infty = \left(\gamma\theta T + \frac{v_0 T^{1-\alpha}}{\Gamma(2-\alpha)} \right) \frac{\sqrt{1-\rho^2}}{\gamma\nu}.$$

If we use the sinh-deformation with the parameters ω_1, b, ω , then, as $\xi \rightarrow \infty$ in the right half-plane along the contour $\mathcal{L}_{\omega_1, b, \omega}$, the absolute value of the integrand admits a bound via $H|\xi|^{-2} \exp(-c_\infty(\omega)|\xi|)$, where H is a constant, and

$$(4.21) \quad c_\infty(\omega) = z_T \sin(\omega) + \operatorname{Re} c_\infty \cos(\omega).$$

Therefore, for a given error tolerance, an approximately optimal ω is found as the maximizer of $c_\infty(\omega)$, and then Λ is chosen solving (approximately, because high accuracy is unnecessary) the equation

$$H \exp[-(c_\infty(\omega)b/2)e^\Lambda] = \epsilon,$$

which gives

$$(4.22) \quad \Lambda = \ln[2 \ln(H/\epsilon) / (bc_\infty(\omega))]$$

and $N = \operatorname{ceil} \Lambda / \epsilon$. If τ is very small or Flat iFT is used, this prescription results in an unnecessary large Λ and N . Then Λ can be decreased solving approximately the equation $H \exp[-(c_\infty(\omega)b/2)e^\Lambda] / \Lambda = \epsilon$. We find (an approximation to) $\Lambda_1 = e^\Lambda$ solving the equation

$$\Lambda_1 = \frac{2}{bc_\infty(\omega)}(\ln \Lambda_1 + E),$$

where $E = \ln(H/\epsilon)$. The following approximation suffices:

$$\Lambda_{10} := 2E/(bc_\infty(\omega)), \quad \Lambda_1 = \frac{2}{bc_\infty(\omega)}(\ln \Lambda_{10} + E), \quad \Lambda_1 := \max\{1.2, \Lambda_1\}.$$

Then we set $\Lambda = \log(\Lambda_1)$, $N = \text{ceil } \Lambda/\zeta$.

4.10. Conformal bootstrap principle. The conformal deformation method (sinh-acceleration in particular) allows one to accurately assess the total error of the method comparing the two prices V^j , $j = 1, 2$, given by (4.18) with two different contour deformations and different N, ζ . If the contours are not close, the terms in one sum are evaluated at points on one curve that are far from the points on the other curve. Hence, if the number of terms is several dozen or more and the difference $V^1 - V^2$ is of the order of 10^{-m} , where $m = 3, 4, \dots$, then the probability (assuming that the prior is the uniform distribution over the non-arbitrage interval) that the difference of the exact (unknown) price V from either of V^1, V^2 is greater than 10^{-m+2} is essentially 0. We used this ad-hoc principle in [17, 19, 22, 21]. In the case of the rough Heston model, the existence of a cone of analyticity is unknown. Although certain results for a strip of analyticity are available [42], the rate of decay of the characteristic function at infinity is unknown. Hence, the scheme applied to the Heston model and affine SV models [51, 52, 17] cannot be justified rigorously, even if the Flat iFT method is applied. In other complicated SV models, the strip (or tube domain in the multi-factor models) and cone of analyticity where the characteristic function decays is also unknown, and difficult to find. To resolve this difficulty, we suggest the following heuristic principle.

CONFORMAL BOOTSTRAP PRINCIPLE I. *Let a union \mathcal{U} of a strip and cone of analyticity of the characteristic function $\Phi(\xi)$ is known, and $\Phi(\xi)$ can be calculated with an (almost) machine precision. Construct at least two admissible conformal deformations of χ_j , $j = 1, \dots, n$, of the line of integration \mathcal{L}^0 such that the contours $\mathcal{L}_j = \chi_j(\mathcal{L}^0)$, $j = 1, \dots, n$, are not close and diverge at infinity, and calculate the approximations V^j to the price using the corresponding changes of variables and simplified trapezoid rule with several dozens of terms and more.*

If $|V^j - V^k| < 10^{-m}$ for $j, k \in 1, \dots, n$, where m is not too small, e.g., $m \geq 5$, then then, as a practical heuristic, the common value can be adopted with a conservative tolerance of order 10^{-m+2} .

Lack of agreement across either contours or procedures should be interpreted as evidence of unresolved numerical/analyticity issues (e.g., contour crossing a latent singularity, insufficient decay, or bias in $\Phi_{ap,r}$), in which case one should refine the discretization, modify the deformations, or increase precision. This is an a posteriori consistency check across independent admissible contours. Agreement across such deformations is taken as evidence that quadrature, tail truncation, and roundoff errors are collectively small; disagreement flags the need to refine the quadrature, enlarge \mathcal{U} , or adjust the deformation.

It is possible that a region of analyticity \mathcal{U} and the rate of decay of $\Phi(\xi)$ as $\xi \rightarrow \infty$ remaining in \mathcal{U} are unknown as well (this is the case for the rough Heston model). Then we use

CONFORMAL BOOTSTRAP PRINCIPLE II. *Assume that we have two or more numerical procedures for evaluation of $\Phi(\xi)$ for ξ in a union \mathcal{U} of a strip and cone. Let $\Phi_{ap,j}(\xi)$, $j = 1, 2$, be the approximations. At least one of the functions $\Phi_{ap,j}$ may not be an analytic function.*

Then, if we use different $\Phi_{ap,j}$ to evaluate the integrals over different contours \mathcal{L}_j , and after the corresponding changes of variables and application of the simplified trapezoid rule with

several dozen of terms and more, the results agree with the accuracy 10^{-m} where m is not small, e.g., $m \geq 7$, then, *as a practical heuristic*, we

- (1) accept that Φ is analytic in a simply connected region $\mathcal{U}_0 \subset \mathcal{U}$ containing the chosen contours;
- (2) the common value can be adopted with a conservative tolerance of order 10^{-m+2} .

Lack of agreement across either contours or procedures should be interpreted as evidence that either one of the deformed contours or both are either outside the domain of analyticity or too close to the boundary, or unresolved numerical/analyticity issues (e.g., contour crossing a latent singularity, insufficient decay, or bias in $\Phi_{ap,r}$), in which case one should modify the deformations. If there is no improvement, the deformations must be changed. When a moderately good agreement is reached, the discretization must be refined and number of nodes increased. If the improvement is observed, the deformed contours are within a domain of analyticity, and we refine the discretization, increase the number of nodes or increase precision to verify that the agreement improves.

Example 4.2. In Table 14, we show the first ten terms in the truncated infinite trapezoid rule for 3 different deformations, when the put price in the rough Heston model with parameters (1.3) is calculated. Spot $S_0 = 1$, strike $K = 0.8$. The resulting put prices are 0.00611179127528501, 0.00611179083570821 and 0.00611179093246816, the number of terms 42, 47 and 41, respectively. The numbers shown in the table are very different, and the sums differences are smaller than $5E - 10$. Hence, the probability that the “true price” differs from the approximations shown by more than e-08 is negligible.

5. NUMERICAL EXAMPLES

The calculations in this section were performed in MATLAB 2024b-academic use, on a MacPro Chip Apple M1 Max Pro chip (3.2-GHz processor) with 10-core CPU, 24-core GPU, 16-core Neural Engine 32GB unified memory, 1TB SSD storage.

5.1. Comparison of the efficiency of different methods for pricing in the Heston model. To avoid the analysis of the potential impact of errors of the Adams method and its modification on the final results, we start with the Heston model, where the integrand can be calculated with machine precision, and, therefore, the errors are the errors of the Fourier inversion method used. In the tables, we show the parameters of each numerical scheme used so that the reader can check that the errors are as shown in the table.

We use [5, Table 2] and prices and relative errors of SINC method shown in [5, Table 2]. Typically, authors tend to select examples to show advantages of their method, hence, we may presume that the authors of [5] believe that the results shown are good. However, we use small relative errors of ITM puts shown in [5, Table 2] to calculate the relative errors of the corresponding OTM call options, which are needed for calibration. The errors of OTM calls turn out to be quite significant, which makes SINC method non-suitable for calibration purposes. In [5, Table 2], the maturity is $T = 0.1$. The results shown in Table 4 clearly demonstrate that, in addition to the fact that the SINC method is unnecessarily complicated and uses non-explicit and unreliable recommendations for the choice of the truncation parameters, it is also significantly slower than Flat iFT with BS correction, the Gauss-Laguerre quadrature and SINH-CB method, and the Gauss-Legendre quadrature is significantly less accurate bar in a

TABLE 4. Benchmark prices [5, Table 2] of OTM and ATM put (panel A) and call (panel B) options calculated using the SINC method in the Heston model with parameters $\kappa = 1.5768, m = 0.0398, \sigma = 0.5751, \rho = -0.5711, v_0 = 0.0175$, and relative errors of several methods w.r.t. to the BB prices calculated using a more accurate SINH-CB method (shown separately). Maturity $T = 0.1$, N is the number of terms of the quadrature.

A K	0.6	0.7	0.8	0.9	1	N
BB_{SINC}	1.1E-09	2.363E-07	1.98699E-05	8.057899E-4	0.0163700005	1024
SINH rel.err.	-4.77E-03	8.73E-06	-9.47E-09	-7.72E-11	-1.65E-11	27-44
Flat iFT-BS	-2.79E-04	4.17E-07	-5.13E-09	1.07E-09	1.08E-10	60
Gauss-Laguerre	8.15E-03	4.33E-05	5.48E-07	1.43E-08	7.39E-10	175
Flat iFT	2.52E-04	7.88E-07	5.82E-08	-3.34E-09	-3.51E-09	200
SINC	-6.16E-02	-2.32E-04	-4.62E-06	-5.84E-08	-2.02E-09	384
	5.36E-01	1.88E-03	5.07E-05	-2.17E-06	8.96E-08	256
Gauss-Kronrod	-1.42E-01	-4.97E-04	2.65E-05	4.57E-05	-4.17E-07	
Gauss-Legendre	4.09E+05	-4.04E+02	3.89E+00	1.01E-02	-9.03E-08	200
B K	1	1.0	1.2	1.3	1.4	N
BB_{SINC}	0.0163700005	6.85530575637E-05	1.223E-07	2.0E-10	0	1024
SINH rel.err.	-1.65E-11	-2.10E-09	1.87E-05	1.17E-03	7.22E+00	44 - 30
Flat iFT-BS	1.08E-10	-3.05E-08	7.74E-06	3.25E-02	1.63E+02	60
Gauss-Laguerre	7.39E-10	1.85E-07	1.09E-04	5.48E-02	2.09E+01	175
Flat iFT	-3.51E-09	7.68E-07	-7.79E-04	-5.38E-01	-1.24E+02	200
SINC	-2.02E-09	-8.40E-07	-6.36E-04	-2.12E-01	-1.00E+00	384
	8.96E-08	2.69E-05	-1.62E-02	-8.09E+00	2.73E+03	256
Gauss-Kronrod	-4.17E-07	-3.89E-05	-6.54E-01	3.81E-02	7.54E+04	
Gauss-Legendre	-9.03E-08	2.48E-02	1.63E+02	3.43E+05	3.26E+08	200

SINH-CB benchmark prices for $K = (0.6 : 0.1 : 1.4)$: 1.17218E - 09; 2.36354837E - 07; 1.9869991862E - 05;

8.057899470805E - 04; 0.0163700005331343; 6.855305756E - 05; 1.22377846E - 07; 2.538235E - 10; 6.968E - 13.

Benchmark prices are calculated using $N = 70 - 110$ terms, absolute errors are smaller than E-15.

The prices and relative errors of ITM put options of SINC method presented in [5, Table 2] are recalculated for the corresponding OTM call options.

Parameters of SINH are chosen using the universal scheme for the error tolerance $E = 10$ with

$\gamma_+ = \pi/2, \gamma_- = 0, \mu_+ = 0, \mu_- = -1$ for puts and $\gamma_+ = 0, \gamma_- = -\pi/2, \gamma_- = 0, \mu_+ = 0, \mu_- = -1$ for calls.

Flat iFT-BS prices are calculated using $\sigma = 0.15, \omega_1 = -0.1, \zeta = 6.7, N = 60$

Flat iFT prices are calculated using $\omega_1 = 9, \zeta = 1, N = 200$.

small vicinity of the spot. Therefore, in the following two tables Table 5 and 6 for $T = 0.5$ and $T = 2$, we do not calculate the errors of SINC method. We also do not show the errors of the Gauss-Legendre quadrature because the errors are systematically and significantly larger than the errors of the Gauss-Laguerre quadrature. The parameters in Tables 4 - 6 are the ones in [5, Table 2], and the riskless and dividend rates $r = 0, q = 0$.

5.2. Performance in “good regions” of the (K, T) -plane. Tables 11, 12 and 13 in Sect. E demonstrate that even in a rather difficult for accurate pricing rough Heston model, in regions not close to maturity and rather close to the spot, a moderately small error tolerance can be satisfied using essentially any reasonable method with a small number of terms, hence, if the data set contains points in this region only, then, for practical purposes, the Gaussian quadratures, Flat iFT, Flat iFT-BM and SINH-CB are essentially equally good. However, since practically useful data sets do contain points in inconvenient regions, significant calibration errors result if either an insufficiently accurate method is used or the parameter choice is not good; if the same parameters are used to calculate option prices for all (K, T) and all parameters of the model, serious errors are inevitable. For similar examples in the context of pricing in KoBoL (a.k.a.) CGMY model, see Tables 15 - 16.

TABLE 5. Benchmark prices of OTM and ATM put (panel A) and call (panel B) options calculated using SINH-CB quadrature, in the Heston model, and relative errors of several methods. Parameters are as in Table 4, maturity $T = 0.5$, N is the number of terms of the quadrature.

A K	0.4	0.6	0.8	1	N
BB_{SINH}	6.867676571E-06	2.88352018707E-04	4.1468390508486E-03	0.0381474566373446	37-59
$SINH$	2.39E-06	2.63E-07	-6.01E-09	-1.52E-11	23-37
Flat iFT-BS	3.89E-07	1.79E-07	2.97E-09	-1.37E-08	70
Gauss-Laguerre	1.20E-06	3.37E-08	2.63E-09	3.17E-10	175
Flat iFT	-3.75E-08	5.07E-09	-1.20E-09	-4.24E-09	200
Gauss-Kronrod	-1.01E-04	2.82E-07	-3.16E-08	-4.66E-07	
K	1	1.2	1.4	1.6	N
BB_{SINH}	0.0381474566373446	8.340111339346E-04	3.28092085119E-05	2.04002697E-06	59-45
$SINH$	-1.52E-11	1.46E-09	-1.97E-08	1.10E-05	37-28
Flat iFT-BS	-1.37E-08	7.90E-07	1.02E-05	1.01E-03	70
Gauss-Laguerre	3.17E-10	1.60E-08	4.42E-07	7.75E-06	175
Flat iFT	-4.24E-09	-2.10E-07	1.62E-05	4.59E-04	200
Gauss-Kronrod	-4.66E-07	2.26E-03	1.87E-03	5.641E-04	

Benchmark prices are calculated using $N = 70 - 110$ terms, absolute errors are smaller than E-15.

Parameters of SINH are chosen using the universal scheme for the error tolerance $E = 10$ with

$\gamma_+ = \pi/2, \gamma_- = 0, \mu_+ = 0, \mu_- = -1$ for puts and $\gamma_+ = 0, \gamma_- = -\pi/2, \gamma_- = 0, \mu_+ = 0, \mu_- = -1$ for calls.

Flat iFT-BS prices are calculated using $\sigma = 0.15, \omega_1 = -0.1, \zeta = 2.5, N = 70$

Flat iFT prices are calculated using $\omega_1 = 5, \zeta = 0.95, N = 200$.

TABLE 6. Benchmark prices of OTM and ATM put (panel A) and call (panel B) options calculated using SINH-CB quadrature, in the Heston model, and relative errors of several methods. Parameters are as in Table 4, maturity $T = 2$, N is the number of terms of the quadrature.

A K	0.4	0.6	0.8	1	N
BB_{SINH}	1.31922212162344E-03	7.65194031130601E-03	0.0290086131558373	0.0886812708686885	34-45
$SINH$	-1.24E-06	4.46E-07	-2.32E-07	-6.36E-08	21-28
Flat iFT-BS	2.56E-08	1.18E-08	1.59E-08	9.86E-09	65
Gauss-Laguerre	7.02E-09	1.19E-09	3.59E-10	1.31E-10	175
Flat iFT	6.56E-10	-2.95E-11	2.178E-11	2.61E-11	200
Gauss-Kronrod	3.64E-05	-1.17E-06	-1.38E-08	-1.07E-09	
K	1	1.2	1.4	1.6	N
BB_{SINH}	0.0886812708686885	0.0198570250501392	0.00387696016670591	9.364368682739E-04	65-61
$SINH$	-6.36E-08	-1.82E-07	3.06E-06	-2.30E-06	28-26
Flat iFT-BS	9.86E-09	9.883E-08	9.62E-07	7.43E-06	70
Gauss-Laguerre	3.17E-10	1.60E-08	4.42E-07	7.75E-06	175
Flat iFT	2.61E-11	2.71E-10	2.31E-09	1.66E-08	200
Gauss-Kronrod	-1.07E-09	-1.40E-08	-3.00E-07	-6.27E-08	

Absolute errors of the benchmark-sinh prices are smaller than E-15

Parameters of SINH are chosen using the universal scheme for the error tolerance $E = 10$ with

$\gamma_+ = \pi/2, \gamma_- = 0, \mu_+ = 0, \mu_- = -1$ for puts and $\gamma_+ = 0, \gamma_- = -\pi/2, \gamma_- = 0, \mu_+ = 0, \mu_- = -1$ for calls.

Flat iFT-BS prices are calculated using $\sigma = 0.15, \omega_1 = -0.1, \zeta = 1.1, N = 65$

Flat iFT prices are calculated using $\omega_1 = 3, \zeta = 0.25, N = 200$.

5.3. Examples of incorrect shapes. In Fig. 8 we show the correct ATM skew for the model with parameters (1.3). It is clearly seen that the skew is more than 2 times lower than the one shown on [34, Fig. 5.1]. The correct implied volatility curves shown on Fig. 9 are essentially straight lines, the slope depending on the maturity, whereas the curves [34, Fig. 5.2] are not so flat, which is expected, and agree with the empirical data well. Recall that in [34], the Lewis method and standard fractional Adams method are used; both are inaccurate. We have

an example of ghost calibration. For the same parameter set, playing with the parameters of the CM method and using interpolation into the bargain, one can produce implied volatility surfaces of different shapes. See Figure 10. In Fig. 11 and 12, we show the correct implied volatility curves for two sets of parameters calibrated to the real data in [27] and [32]. The curves shown in [32] differ by several percent and more, hence, we have an additional pair of ghost calibration examples.

6. FAST PRICING

6.1. Pricing algorithms. We give a detailed description of the pricing algorithm based on the Conformal Bootstrap principle, the sinh-deformation of the contour, and the modified Adams method. There are two versions of the algorithm: one which is used to calculate the benchmarks, and a faster one to be used on the fly, e.g. during calibration or for live pricing. The detailed description of the benchmark pricing algorithm can be found in Appendix C.

6.2. Calibration pricer. The on-the-fly pricing algorithm used during the calibration is similar to the one outlined in Appendix C, except that the time-consuming optimization is not used, and the flat contour price $V_{LL}(T, K)$ (cf. (4.9)) is only calculated when necessary. We proceed as follows

1. Take a strip of analyticity, e.g. $(0, \pi/4)$ (see Step II in section 4.8 for the choice of the strip).
2. In a loop, price all OTM puts or calls using $\omega = 0.1, 0.2, \dots$, at each step, e.g. using an initial number of $M = 100$ timesteps in the Adams method for $T > 1$, and $M = 300$ for $T < 1$. The modification of section 3.2 is used.
3. The procedure described in Appendix C.3 is used, which successively adjusts the numerical parameters (number of timesteps M , truncation parameter Λ , mesh ζ , number of iterations n in the modified Adams method) by adjusting each until further refinement has negligible effect.
4. Exit the loop as soon as any two prices have relative difference under e.g. $2 \cdot 10^{-5}$, and return the last price.
5. Otherwise, try a similar loop with a larger initial value of M , e.g. $M = 500$.
6. If no convergence is observed, then calculate the price along a flat contour with $\text{Im } \xi = -0.5$, large initial value of M , e.g. $M = 1000$, and no sinh deformation (i.e. using the Lewis-Lipton formula), and check the relative differences between this and any of the previous set of prices.

6.3. Performance times.

6.3.1. Hardware and software environment. All benchmarks were executed on a dual-socket AMD EPYC 7H12 server (2×64 physical cores, 256 hardware threads, max boost 2.60 GHz) running Ubuntu 22.04.5 LTS with the Linux 5.15.0-130-generic kernel. The machine was equipped with 256 GB DDR4-3200 RAM. Primary storage comprised a 447 GB RAID-1 Intel SSD system volume. No GPU or other hardware accelerators were employed; all timings reported in this paper refer to this CPU-only configuration.

6.3.2. *Implementation details.* The rough-Heston pricer uses a fully vectorised implementation of the Adams method that is *just-in-time* compiled with `numba`. The vanilla-Heston benchmark, by contrast, is a pure Python/NumPy implementation of algorithm in [28], does not employ `numba`, and sets the roughness parameter to the classical value $\alpha = 1$ (i.e. $H = 1/2$).

6.3.3. *Measured timings.* Table 7 reports the mean wall-clock time required to price a single ATM European put option with expiry⁶ $T = 2/365$ under each parameter set. We used $\omega = 0.1$. Times were obtained with Python’s `cProfile`, using the high-resolution `perf_counter` timer. For each parameter set we performed one warm-up call, to trigger `numba` compilation where applicable, followed by 1000 pricing calls; the value shown is the profiler’s cumulative time divided by the number of calls. The results indicate near-parity between the two models for the El Euch-Rosenbaum (EuRos) and SPY sets (24 ms vs. 23 ms and 30 ms vs. 19 ms, respectively), whereas for the higher-volatility TSLA and MSTR sets the rough model is roughly 2–5 times slower.

6.3.4. *Expected performance in vectorised C++.* If both pricers were re-implemented in high-performance, vectorised C++ with identical numerical tolerances, the Python overhead would disappear and both methods would be expected to complete in a few milliseconds per price evaluation. Since the rough-Heston characteristic function involves the additional application of the Adams method, practical experience suggests that the rough model would then run roughly 1–5 times slower than the vanilla Heston pricer.

6.3.5. *Comparison with Markovian approximation.* Table 8 reports the total pricing times for the same parameter sets, for an ATM put option and for maturities of 2 days and 1 week. Prices were obtained using the BL2 method, identified in [7] as the most efficient and accurate one among the proposed approaches. In (2.17), the number of nodes n was selected so that the ATM volatility error remained under 1%. The timings were obtained by running the Python implementation made available by the authors of [7] on GitHub [24]. Less than 2% of the total runtime is spent on node computation, leaving little room for acceleration through pre-caching. A full description of the algorithm can be found in Appendix D. We used a tolerance of $\varepsilon = 10^{-3}$ for the relative error.

TABLE 7. Average wall-clock time per contract for the rough and vanilla Heston pricers on the hardware described above.⁷

Set	Rough Heston (ms)	Vanilla Heston (ms)
EuRos	24	23
TSLA	50	19
MSTR	91	20
SPY	30	19

⁶In this section and in the following one, we use calendar days (e.g. $T = 2/365$), as commonly done by practitioners, since expiry is a calendar date, carry (rates/dividends/borrow) accrues in calendar time, and weekend theta/P&L is realized. For short maturities the difference can be material. The academic literature often uses 252 trading days.

TABLE 8. Calculation times for the BL2 Markovian approximation method [7], based on the minimal number of nodes n in (2.17) needed to keep the ATM volatility error below 1%

Set	Expiry	Nodes	Time (sec.)
TSLA	2D	2	51.89
TSLA	1W	2	16.77
MSTR	2D	1	3.90
MSTR	1W	1	1.58
EuRos	2D	1	4.11
EuRos	1W	1	2.79
SPY	2D	1	1.57
SPY	1W	1	0.83

7. CALIBRATION RESULTS

7.1. Calibration using SINH-CB. This section includes an example of how our new pricing method can be applied to calibrate the rough Heston model, using Tesla (TSLA) option data from Bloomberg. We perform the calibration on TSLA implied volatility smiles as of 2 May 2025, fitting on short-dated maturities (1-week and 2-week expiries), by minimising the sum of squared differences between model and market implied volatilities. Figure 5 below shows the in-sample fit of the model to market implied volatilities for these maturities. The rough Heston model is able to closely reproduce the observed smiles at 1-week and 2-week expiries.

To verify the reliability of the fast pricer used in our calibration procedure, we conducted a “reverse calibration” test. In this test, we used the benchmark pricer described in Appendix C and the set of calibrated parameters, i.e.

$$(\alpha, \gamma, \theta, \sigma, \rho, v_0) = (0.511913, 2.36609, 0.424949, 1.36839, -0.178493, 0.527527),$$

where $\sigma = \gamma\nu$, to generate option prices, hence and implied vols, at expiries corresponding to 4, 11, 17 and 25 days, respectively, and moneyness levels between 0.6 and 1.6 for the first two expiries, and between 0.4 and 1.75 for the others. Treating these as “market” quotes, we then recalibrated the model with our fast pricer (described in section 6.2). The latter recovered virtually identical parameters:

$$(\alpha, \gamma, \theta, \sigma, \rho, v_0)_{\text{fast}} = (0.512399, 2.38011, 0.425275, 1.37226, -0.178501, 0.527526).$$

These match the benchmark values within about 0.2% on every parameter. The maximum absolute deviation in any parameter is only 1.4×10^{-3} (occurring in the mean-reversion rate γ , which is the hardest to calibrate), and the average relative error is approximately 0.08%.

⁷Vanilla Heston prices were computed with the method of [28] (no `numba` acceleration) and use $\alpha = 1$ ($H = 1/2$). The TSLA set was calculated to options on this name as of 2 May 2025 (cf. Section 7), while MSTR and SPY were calibrated to the corresponding names as of 2 June and 31 March, 2025, respectively. The parameter sets are as follows, with $\sigma = \gamma\nu$; $(\alpha, \gamma, \theta, \sigma, \rho, v_0)$: EuRos $(0.62, 0.10, 0.3156, 0.0331, -0.681, 0.0392)$ from [34, §5.2]; TSLA $(0.5119, 2.3661, 0.4249, 1.3684, -0.1785, 0.5275)$; MSTR $(0.6254, 2.2046, 1.1908, 3.9948, -0.4078, 0.3458)$; SPY $(0.7151, 1.8967, 0.03848, 1.1654, -0.6704, 0.06246)$.

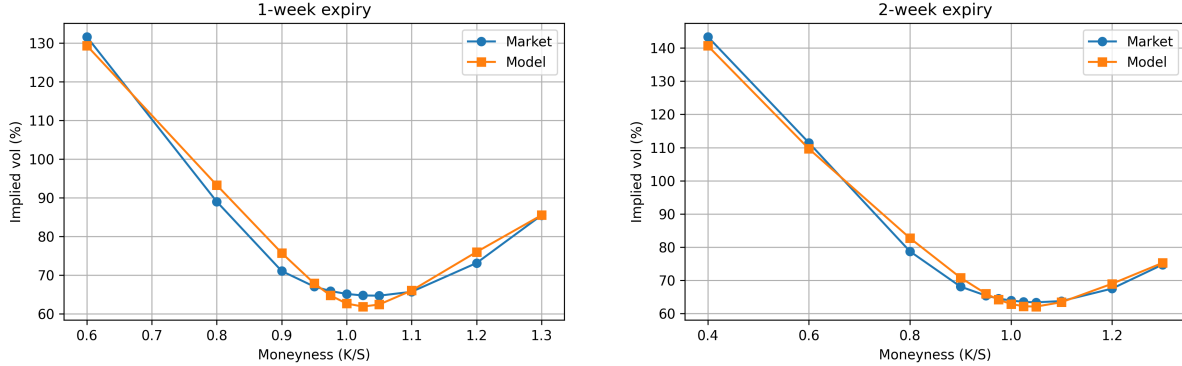


FIGURE 5. In-sample calibration of the rough Heston model to TSLA option smiles on 2 May 2025. Implied volatility (IV) smiles for the 1-week expiry (left panel) and 2-week expiry (right panel) are shown. Market IVs (blue) are closely fitted by the model IVs (orange).

These results confirm that the our fast pricer, based on conformal bootstrapping with sinh-deformation, is sufficiently accurate and robust for calibration, essentially reproducing the original model parameters.

Aside from the pricer's performance, we also find that the model calibration extrapolates well across time. Using the parameters calibrated to the 1W–2W expiries, we priced options at longer maturities that were not included in the calibration (3W and 4W expiries). The resulting implied volatility smiles, shown in Figure 6, indicate that the model's predictions remain close to the actual market smiles for these longer expiries. In other words, the rough Heston model calibrated to short-term options is able to capture the term structure of volatility out to about one month without any re-calibration. This is especially useful for applications to market making, since broker dealers or market makers often need to provide quotes for illiquid expiries.

In order to assess the calibration quality in a way familiar to practitioners, we follow the “average percentage error” (APE) definition of [60] and apply the same statistic directly to implied volatilities.⁸ The resulting *average volatility error* (AVE) at a given expiry is

$$(7.1) \quad \text{AVE} = \frac{\frac{1}{N} \sum_{i=1}^N |\sigma_i^{\text{mkt}} - \sigma_i^{\text{model}}|}{\overline{\sigma^{\text{mkt}}}} \times 100\%,$$

where N is the number of strikes in the plot and $\overline{\sigma^{\text{mkt}}}$ is the strike-averaged market IV.

Table 9 below lists the AVE values corresponding to the smiles shown in Figures 5 - 6.

The AVE stays well below 3% even at five months' expiry, indicating robust extrapolation across maturities.

⁸The original paper defines APE for option prices.

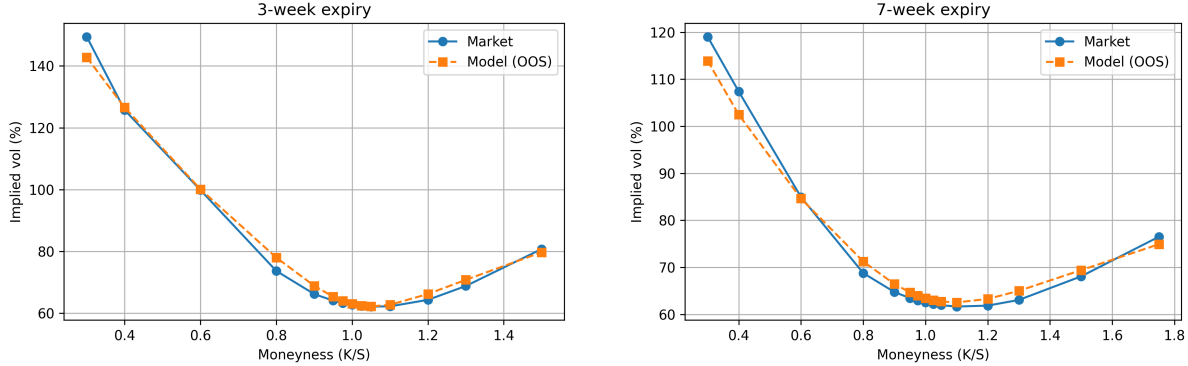


FIGURE 6. Out-of-sample implied volatility smiles at longer expiries on 2 May 2025, using the rough Heston parameters calibrated only on 1–2 week maturities. The model (orange lines) extrapolates the smile well for both the 3-week expiry (left) and 7-week expiry (right), staying in line with the market implied volatilities (blue lines). This demonstrates the model’s robust extrapolation in the near-term maturity range.

TABLE 9. Average Volatility Error (AVE) by maturity, computed with Eq. (7.1).

Expiry	Strike range	AVE (%)
1 week	$0.40 \leq K/S \leq 1.30$	2.85
2 weeks	$0.40 \leq K/S \leq 1.30$	1.95
3 weeks	$0.30 \leq K/S \leq 1.50$	2.04
7 weeks	$0.30 \leq K/S \leq 1.75$	2.43
5 months	$0.30 \leq K/S \leq 2.50$	1.96

7.2. Calibration pitfalls. We show the consequences on the calibration results of using fixed pricing settings, as often done by practitioners and academics alike, e.g. when using CM, COS, or even Gaussian quadratures. We compare the calibration results obtained in the previous section with those obtained using Gauss-Laguerre quadrature with $N = 200$ nodes, and $M = 1000$ time steps in the Adams method, which is higher than the value of M used for SINH-CB for any of the calibrations described in the previous section. The same modification of the Adams method is used as for SINH-CB, and the model is calibrated to the same implied volatilities for 1W and 2W expiries, as in section 7.1. The resulting parameters are

$$(\alpha, \gamma, \theta, \sigma, \rho, v_0)_{\text{GL}} = (0.587271, 3.22767, 0.219608, 1.49494, -0.310089, 0.552303).$$

The maximum absolute deviation in any parameter is 48.3%, for θ , and the average deviation is 31.2%. Figure 7 below shows the pitfalls of inaccurate pricing in model calibration. The left panel shows the “ghost calibration” effect: the solid red line is the 1W implied volatility calculated from the model parameters above, which appears to fit the market, however this is an illusion. When the model’s true volatility curve is calculated using SINH-CB (dashed

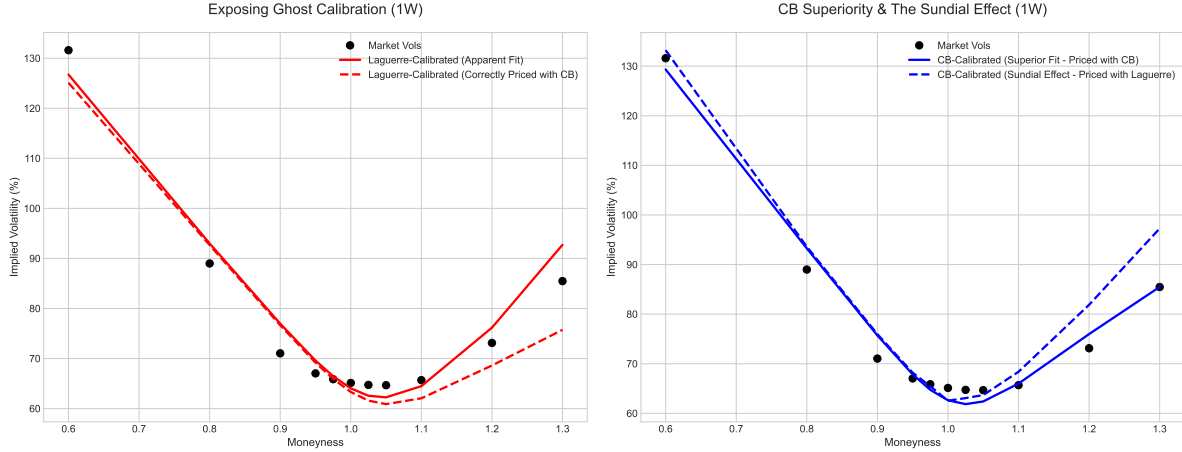


FIGURE 7. Calibrated 1W smiles with the rough Heston model to 1W and 2W TSLA implied vols on 2 May 2025, using Gauss-Laguerre with 200 nodes and 1000 Adams time steps. Left panel: GL pricer produces a model that appears to fit the market (solid red line); the dashed red line shows the actual volatility curve calculated from the same parameters. Right panel: GL pricer fails to price accurately the superior fit to the market data.

red line), it is revealed to be a poor match. The right panel shows the “sundial effect”: our proposed SINH-CB method finds a superior fit to the market (solid blue line). If one tries to use the GL pricer on this superior model, it fails to reproduce the correct volatilities, especially in the right tail. This shows how a flawed tool can cause a good model to be incorrectly dismissed.

8. CONCLUSION

In the paper, we constructed the accurate and fast SINH-CB method for the pricing of European options in the rough Heston model, amenable to automatic and efficient error control. The main ingredients are: 1) an appropriate conformal deformation of the contour of integration in the Fourier inversion formula, followed by the corresponding conformal change of variables and application of the simplified trapezoid rule (sinh-acceleration); 2) a modification of the fractional Adams method, which is a crucial improvement in the presence of a large spectral parameter; 3) an ad-hoc Conformal Bootstrap principle: if the prices obtained with two deformations differ by less than 10^{-m} , where $m \geq 5$, then the probability (assuming that the prior is a uniform distribution over the no-arbitrage interval) that either of the prices differs from the correct price (calculated using a perfect pricer) by more than 10^{-m+2} is negligible.⁹ Using the pricer, we constructed a novel fast and accurate calibration scheme, and applied the scheme to calibration of the rough Heston model to the real data. The calibration scheme satisfies all the requirements needed for practical applications. The pricing needs to take calculation times of the order of a millisecond in a production environment, which usually corresponds to a few tens of a millisecond, when implemented in Python on a home PC, without compilation

⁹Ingredients 1) and 3) can be used in calibration procedures of any model where the Fourier transform technique is used

or optimisation. Moreover, as noted in [28], the calculation needs to be extremely accurate, in order to cope with both very long and very short maturities, and with options which are very far in and out of the money, for a wide range of model parameters that can result from calibration to market data. This is especially true in the context of regulatory counterparty credit risk, where exposure profiles are effectivised¹⁰ and therefore any large errors which occur during the Monte Carlo simulation can propagate across time. In recent years, a growing body of literature has explored the use of machine learning (ML) techniques, particularly deep neural networks, to accelerate pricing and calibration under rough volatility. Horvath, Muguruza, and Tomas [44], as well as Bayer, Horvath, and Stemper [10], have introduced deep learning approaches to approximate the pricing map in rough Bergomi and rough Heston models, which are sufficiently fast for real-time calibration. However, such methods suffer from one common drawback: in addition to speed, banks must ensure accuracy, transparency, and stability for such methods to be used in pricing, hedging, and risk management, especially in models subject to regulatory approval. For example, the Federal Reserve's SR 11-7 regulatory standard for model validation, which is used in most sell-side institutions, asks to perform critical analyses to determine the model's assumptions and limitations, as well as to “*establish the boundaries of model performance by identifying the acceptable range of inputs as well as conditions under which the model may become unstable or inaccurate*” [57]. Clearly, this is extremely challenging for a black-box pricer.

The fast reliable SINH-CB method (sinh-acceleration - conformal bootstrap) constructed in the paper is significantly faster than other methods and satisfies all the requirements above whereas popular methods are either too slow or inaccurate or unreliable. In our numerical experiments, the SINH-CB method demonstrated a sufficiently good accuracy for calibration purposes if the OTM option prices larger than $E - 07$ of the spot price S_0 were used. Some of the popular methods work fairly well in a narrower region of the strike-maturity (K, T) - plane *provided the parameters of the scheme are chosen correctly* but are slower and not so reliable; other methods are rather inaccurate in wide regions in the (K, T) plane, which leads to very inaccurate prices and implied volatility curves. Following Leo Tolstoy (“All happy families are alike; each unhappy family is unhappy in its own way”), we can formulate the *Anna Karenina principle for option pricing*: in a good region of (K, T) -space, all reasonable models and pricing methods are alike; close/far from maturity and far in the tails, models and pricing methods perform differently¹¹. Our numerical experiments demonstrate that SINH-CB method satisfies all the requirements better than other methods, followed by a simple modification of the standard Fourier inversion method (Flat iFT with the BM correction); the Gauss-Laguerre method requires 2-5 times more terms than SINH-CB to achieve the accuracy sufficient for applications. If the number of nodes needs to be increased, then all values of the integrand needs to be recalculated whereas in the case SINH-CB, only a small number of additional terms need to be calculated. In the case of the rough Heston model, the evaluation of the integrand at chosen nodes is very time consuming, hence, SINH-BC has an additional

¹⁰For capital requirements, the “Effective Expected Positive Exposure” is set equal to $\text{EEPE} = \sup_{t \in [0, T]} \mathbb{E}[\max(V_t, 0)]$, where V_t is the time- t portfolio value.

¹¹Disclaimer: we are not the first to formulate the principle. J. Diamond [29] formulated the principle in applications to biology: “A deficiency in any one of a great number of factors can render a species undomesticable. Therefore, all successfully domesticated species are not so because of a particular positive trait, but because of a lack of any number of possible negative traits.”

advantage. We explained the sources of instability of the Gauss-Laguerre quadrature and COS and SINC method. The Gauss-Laguerre quadrature is potentially unstable (and not mathematically justified) if the rate of decay of the integrand is small, which may happen for short maturity options in the Heston model (presumably, in the rough Heston model as well), and COS and SINC method use unreliable recommendations for the choice of the truncation parameter.

We also showed that even if the pricer is sound, one cannot hope to use the same parameters of the numerical scheme for all (K, T) in the data set and all parameters of the model; the number of terms in the Fourier inversion formula and step in the modified Adams method needed to satisfy the desired error tolerance can significantly increase and decrease, respectively. We demonstrated that an unstable and/or inaccurate pricer produces spurious wings of volatility curves, and the shape of the surface may strongly depend on the choice of the parameters of the numerical scheme. We can formulate THE UNCERTAINTY PRINCIPLE OF CALIBRATION: using different parameters of the numerical scheme, one can produce a host of different prices and volatility curves and surfaces, and choose shapes one likes better.

Finally, using the calibration method developed in the paper, we showed that the rough Heston model with a very small Hurst index $H = 0.012$ gives a very good fit (both in and out of the sample) calibrated to options on Tesla stock of maturities 1W-2W; the performance remains equally good out of the sample (maturities 3W and 4W). We also demonstrated how pricing algorithms with fixed, seemingly conservative numerical settings can generate erroneous calibration parameters. These numerical errors can, in turn, lead to the incorrect dismissal of a valid model.

REFERENCES

- [1] M. Abramowitz and I. Stegun. *Handbook of Mathematical Functions, with Formulas, Graphs and Mathematical Tables*. Dover Publications, Mineola, NY, 1965.
- [2] A. Alfonsi and A. Kebaier. Approximation of stochastic volterra equations with kernels of completely monotone type. *Mathematics of Computation*, 93:643–677, 2024. Available at <https://arxiv.org/abs/2102.13505>.
- [3] O.E. Barndorff-Nielsen. Processes of Normal Inverse Gaussian Type. *Finance and Stochastics*, 2:41–68, 1998.
- [4] O.E. Barndorff-Nielsen and S.Z. Levendorskiĭ. Feller Processes of Normal Inverse Gaussian type. *Quantitative Finance*, 1:318–331, 2001.
- [5] F. Baschetti, G. Bormetti, S. Romagnoli, and P. Rossi. The SINC way: a fast and accurate approach to Fourier pricing. *Quantitative Finance*, 22(3):426–446, 2022.
- [6] C. Bayer and S. Breneis. Markovian approximations of stochastic Volterra equations with the fractional kernel. *Quantitative Finance*, 23(1):53–70, 2023. Available at <https://arxiv.org/abs/2108.05048>.
- [7] C. Bayer and S. Breneis. Weak markovian approximations of rough Heston, September 2023. Available at <https://arxiv.org/abs/2309.07023>.
- [8] C. Bayer, P. Fritz, and J. Gatheral. Pricing under rough volatility. *Quantitative Finance*, 15(1):1–18, 2015.
- [9] C. Bayer, P.K. Friz, M. Fukasawa, J. Gatheral, A. Jacquier, and M. Rosenbaum. *Rough volatility*. SIAM, Philadelphia, PA, 2024.
- [10] C. Bayer, B. Horvath, and B. Stemper. On deep calibration of rough stochastic volatility models. *Quantitative Finance*, 21(3):419–437, 2021.
- [11] M. Boyarchenko and S. Levendorskiĭ. Ghost Calibration and Pricing Barrier Options and Credit Default Swaps in spectrally one-sided Lévy models: The Parabolic Laplace Inversion Method. *Quantitative Finance*, 15(3):421–441, 2015. Available at SSRN: <http://ssrn.com/abstract=2445318>.

- [12] S. Boyarchenko and S. Levendorskiĭ. On rational pricing of derivative securities for a family of non-Gaussian processes. Preprint 98/7, Institut für Mathematik, Universität Potsdam, January 1998. Available at <http://opus.kobv.de/ubp/volltexte/2008/2519>.
- [13] S. Boyarchenko and S. Levendorskiĭ. Generalizations of the Black-Scholes equation for truncated Lévy processes. Working Paper, University of Pennsylvania, April 1999.
- [14] S. Boyarchenko and S. Levendorskiĭ. Option pricing for truncated Lévy processes. *International Journal of Theoretical and Applied Finance*, 3(3):549–552, July 2000.
- [15] S. Boyarchenko and S. Levendorskiĭ. New efficient versions of Fourier transform method in applications to option pricing. Working paper, 2011. Available at SSRN: <http://ssrn.com/abstract=1846633>.
- [16] S. Boyarchenko and S. Levendorskiĭ. Efficient variations of Fourier transform in applications to option pricing. *Journal of Computational Finance*, 18(2):57–90, 2014. Available at <http://ssrn.com/abstract=1673034>.
- [17] S. Boyarchenko and S. Levendorskiĭ. Sinh-acceleration: Efficient evaluation of probability distributions, option pricing, and Monte-Carlo simulations. *International Journal of Theoretical and Applied Finance*, 22(3):1950–011, 2019. DOI: 10.1142/S0219024919500110. Available at SSRN: <https://ssrn.com/abstract=3129881> or <http://dx.doi.org/10.2139/ssrn.3129881>.
- [18] S. Boyarchenko and S. Levendorskiĭ. Conformal accelerations method and efficient evaluation of stable distributions. *Acta Applicandae Mathematicae*, 169:711–765, 2020. Available at SSRN: <https://ssrn.com/abstract=3206696> or <http://dx.doi.org/10.2139/ssrn.3206696>.
- [19] S. Boyarchenko and S. Levendorskiĭ. Static and semi-static hedging as contrarian or conformist bets. *Mathematical Finance*, 3(30):921–960, 2020. Available at SSRN: <https://ssrn.com/abstract=3329694> or <http://arXiv.org/abs/1902.02854>.
- [20] S. Boyarchenko and S. Levendorskiĭ. Alternative models for FX, arbitrage opportunities and efficient pricing of double barrier options in Lévy models with memory. Working paper, March 2024. Available at <https://ssrn.com/abstract=46738420> or <http://arxiv.org/abs/2402.16724>.
- [21] S. Boyarchenko and S. Levendorskiĭ. Efficient evaluation of double barrier options. *International Journal of Theoretical and Applied Finance*, 27(2):2450007, 2024. Available at SSRN: <http://ssrn.com/abstract=4262396> or <http://arxiv.org/abs/2211.07765>.
- [22] S. Boyarchenko and S. Levendorskiĭ. Efficient evaluation of expectations of functions of a Lévy process and its extremum. *Finance and Stochastics*, 29:443–468, 2025. Working paper version is available at SSRN: <https://ssrn.com/abstract=4140462> or <http://arXiv.org/abs/2209.02793>.
- [23] S. Boyarchenko and S. Levendorskiĭ. Efficient inverse Z-transform and pricing barrier and lookback options with discrete monitoring. *Frontiers of Mathematical Finance*, 5:140–141, 2025.
- [24] S. Breneis. Approximations to Fractional Stochastic Volterra Equations. https://github.com/SimonBreneis/approximations_to_fractional_stochastic_volterra_equations. Accessed: 17 August 2025.
- [25] G. Callegaro, M. Grasselli, and G. Pagès. Fast Hybrid Schemes for Fractional Riccati Equations (Rough is not so Tough). *Mathematics of Operations Research. Articles in advance*, 46:1–34, 2020.
- [26] P. Carr and D.B. Madan. Option valuation using the Fast Fourier Transform. *Journal of Computational Finance*, 2(4):61–73, 1999.
- [27] P.-A. Coprechot. Study of the joint S&P 500/VIX smile calibration problem within rough volatility models. MSc Thesis, Department of Mathematics, Imperial College, London, 2020.
- [28] M. de Innocentis and S. Levendorskiĭ. Calibration Heston Model for Credit Risk. *Risk*, pages 90–95, September 2017. Available at SSRN: <http://ssrn.com/abstract=2757008>.
- [29] J. Diamond. Zebras and the Anna Karenina principle. *Natural History*, 103(9):4–10, 2014.
- [30] D.LJ. Djukić, R. M.M. Djukić, A.V. Pejčev, and M.M. Spalević. Error estimates of Gaussian-type quadrature formulae for analytic functions on ellipses - a survey of recent results. *Electronic Transactions on Numerical Analysis*, 53:352–382, 1920.
- [31] D. Duffie, D. Filipović, and K. Singleton. Affine processes and applications in finance. *Annals of Applied Probability*, 13:984–1053, 2002.
- [32] K.E. Erkan. European option pricing under the rough Heston model using the COS method. Master thesis. Delft University of Technology, 2020. Available at <https://repository.tudelft.nl/record/uuid:721510e7-6393-4b5e-af07-75063ced210c>.

- [33] O.E. Euch and M. Rosenbaum. Perfect hedging in rough Heston models. Working paper, 2017. Available online at: <https://arxiv.org/abs/1703.05049>.
- [34] O.E. Euch and M. Rosenbaum. The characteristic function of rough Heston models. *Mathematical Finance*, 29:3–38, 2019.
- [35] F. Fang and C.W. Oosterlee. A novel pricing method for European options based on Fourier-Cosine series expansions. *SIAM Journal on Scientific Computing*, 31(2):826–848, 2008.
- [36] L. Feng and V. Linetsky. Pricing discretely monitored barrier options and defaultable bonds in Lévy process models: a fast Hilbert transform approach. *Mathematical Finance*, 18(3):337–384, July 2008.
- [37] M. Forde, B. Smith, and L. Viitasaari. Rough volatility and CGMY jumps with a finite history and the rough Heston model - Small time asymptotics in the $k = \sqrt{t}$ regime. *Quantitative Finance*, 21(4):541–563, 2021.
- [38] M. Forde and H. Zhang. Asymptotics for rough stochastic volatility models. *SIAM J. Financial Mathematics*, 8(1):114–145, 2017.
- [39] P.K. Friz, P. Gassiat, and P. Pigato. Precise asymptotics: Robust stochastic volatility models. *Ann. Appl. Probability*, 31(2):896–940, 2021.
- [40] P.K. Friz, P. Gassiat, and P. Pigato. Short-dated smile under rough volatility: Asymptotics and numerics. *Quantitative Finance*, 22(3):463–480, 2022.
- [41] J. Gatheral, T. Jaisson, and M. Rosenbaum. Volatility is rough. *Quantitative Finance*, 18(6):933–949, 2018.
- [42] S. Gerhold, C. Gerstenecker, and A. Pinter. Moment explosions in the rough Heston model. *Decisions in Economics and Finance*, 42(2):575–608, 2019.
- [43] S. L. Heston. A closed-form solution for options with stochastic volatility with applications to bond and currency options. *The Review of Financial Studies*, 6(2):327–343, 1993.
- [44] B. Horvath, A. Muguruza, M. Roome, and F. Shi. Deep learning volatility. *Quantitative Finance*, 21(1):11–21, 2021.
- [45] E. Abi Jaber, O. El Euch, M. Rosenbaum, and J. Touzi. Markovian structure of the Volterra Heston model. *Mathematical Finance*, 29(3):1080–1108, 2019.
- [46] E. Abi Jaber and O. El Euch. Multifactor approximation of rough volatility models. *SIAM Journal on Financial Mathematics*, 10(2):309–349, 2019.
- [47] E. Abi Jaber, M. Larsson, and S. Pulido. Affine Volterra processes. *Ann. Appl. Probab.*, 29(5):3155–3200, 2019.
- [48] E. Abi Jaber and S. Li. Volatility models in practice: Rough, Path-dependent or Markovian. Working paper, January 2024. Available online at: <https://arxiv.org/abs/2401.03345>.
- [49] A. Jacquier, C. Martini, and A. Muguruza. Pricing under rough volatility. *Quantitative Finance*, 18(1):45–61, 2018.
- [50] R. Lee. Option pricing by Transform methods: Extensions, Unification, and Error control. *Journal of Computational Finance*, 7(3):51–86, 2004.
- [51] S. Levendorskii. Efficient pricing and reliable calibration in the Heston model. *International Journal of Theoretical and Applied Finance*, 15(7), 2012. 125050 (44 pages).
- [52] S. Levendorskii. Pitfalls of the Fourier Transform method in Affine Models, and remedies. *Applied Mathematical Finance*, 23(2):81–134, 2016. Available at <http://dx.doi.org/10.1080/1350486X.2016.1159918> or <http://ssrn.com/abstract=2367547>.
- [53] A. Lewis. A simple option formula for general jump-diffusion and other exponential Lévy processes, September 2001. Available at: <http://papers.ssrn.com/abstract=585451>.
- [54] Alan L. Lewis. *Option valuation under stochastic volatility: with Mathematica code*. Finance Press, Newport, 2000.
- [55] A. Lipton. *Mathematical Methods For Foreign Exchange: A Financial Engineer's Approach*. World Scientific, Singapore, 2001.
- [56] V. Lucic. On singularities in the Heston model. In J. Gatheral, A. Gulisashvili, J. Teichman, P. Friz, and A. Jacquier, editors, *Large Deviations and Asymptotic Methods in Finance*, pages 439–448. Springer, Cham, Heidelberg, New York, Dordrecht, London, 2015. Available at <http://ssrn.com/abstract=1031222>.
- [57] Board of Governors of the Federal Reserve System. SR 11-7: Guidance on model risk management. <https://www.federalreserve.gov/supervisionreg/srletters/sr1107.htm>, 2011. Supervisory Letter SR 11-7, April 4, 2011.

- [58] G. Pagès. Multi-step Richardson-Romberg extrapolation: Remarks on variance control and complexity. *Monte Carlo Methods Appl.*, 13(1):37–70, 2007. <https://arxiv.org/abs/1901.09647>.
- [59] S.I. Romer. Empirical analysis of rough and classical stochastic volatility models to the SPX and VIX markets. *Quantitative Finance*, 22(10):1805–1838, 2022.
- [60] W. Schoutens, E. Simons, and J. Tistaert. A perfect calibration! Now what? *Wilmott Magazine*, pages 66–78, March 2004.
- [61] F. Stenger. *Numerical Methods based on Sinc and Analytic functions*. Springer-Verlag, New York, 1993.
- [62] L. N. Trefethen and J. A. C. Weideman. The exponentially convergent trapezoidal rule. *SIAM Review*, 56(3):385–458, 2014.
- [63] Y. Wang and Z. Cui. Rough Heston model as the scaling limit of bivariate cumulative heavy-tailed INAR(∞) processes and applications. Working paper, April 2025. Available online at: <http://arxiv.org/pdf/2503.18259.pdf>.

APPENDIX A.

A.1. Grids depending on ξ . The accuracy of calculations can be increased using grids depending on ξ . To understand what a proper dependence of the grid on a (large in absolute value) ξ is, we take $\xi = re^{i\varphi}$, where $r \gg 1$ and $\varphi \in (-\pi/4, \pi/4)$. Set $t_1 = tr^{1/\alpha}$, $h_1(r, \varphi, t_1) = r^{-1}h(re^{i\varphi}, t_1 r^{-1/\alpha})$, substitute $t = t_1 r^{-1/\alpha}$ and $h(\xi, t) = rh_1(r, \varphi, t_1)$ into (2.9) and change the variable $s = r^{-1/\alpha} s_1$. We obtain the Volterra equation for h_1 :

$$(A.1) \quad h_1(r, \varphi, t_1) = \frac{1}{\Gamma(\alpha)} \int_0^{t_1} (t_1 - s_1)^{\alpha-1} F_1(r, \varphi, h_1(r, \varphi, s_1)) ds_1,$$

where

$$(A.2) \quad F_1(r, \varphi, h_1) = -\frac{1}{2}(e^{i2\varphi} + ie^{i\varphi}r^{-1}) + \gamma(ie^{i\varphi}\rho\nu - r^{-1})h_1 + \frac{(\gamma\nu)^2}{2}h_1^2.$$

Since $F_1(r, \varphi, h_1)$ is uniformly bounded as a function of r , the equation (A.1) can be integrated accurately if t_1 is not too large; if t_1 is large, the interpolation errors accumulate. Therefore, in a region $t \leq A|\xi|^{-1/\alpha}$, where A is moderately large, we solve (2.9) using a grid with the step of the order of $|\xi|^{-1/\alpha}$, and in the region $t \in [A|\xi|^{-1/\alpha}, T]$, we use a grid independent of ξ .¹² This requires the straightforward recalculation of the coefficients in fractional Adams procedures:

For $k = 0, 1, \dots, M_\xi - 1$ and $j = 0, 1, \dots, k$, calculate

$$\begin{aligned} a_{k+1, k+1} &= \frac{1}{\Gamma(\alpha+2)}(t_{k+1} - t_k)^\alpha, \\ a_{0, k+1} &= \frac{1}{\Gamma(\alpha+2)}((\alpha+1)t_k^\alpha + \frac{1}{t_1}((t_{k+1} - t_1)^{\alpha+1} - t_{k+1}^{\alpha+1})), \end{aligned}$$

and, in the cycle $j = 1, 1, \dots, k$, calculate

$$\begin{aligned} a_{j, k+1} &= \frac{1}{\Gamma(\alpha+2)} \left\{ \frac{(t_{k+1} - t_{j-1})^{\alpha+1}}{t_j - t_{j-1}} + \frac{(t_{k+1} - t_{j+1})^{\alpha+1}}{t_{j+1} - t_j} \right. \\ &\quad \left. - (t_{k+1} - t_j)^{\alpha+1} \left[\frac{1}{t_{j+1} - t_j} + \frac{1}{t_j - t_{j-1}} \right] \right\} \end{aligned}$$

¹²We construct grids that are unions of two uniform grids for simplicity. One can use more complicated grids. The only essential requirement is that the step on $[0, A|\xi|^{-1/\alpha}]$ must be much finer than the ones on $[A|\xi|^{-1/\alpha}, T]$.

APPENDIX B. PSEUDO-CODE IMPLEMENTATION OF THE BL MODIFICATION OF THE ADAMS METHOD

This section gives a scheme for the implementation of the BL-modified Adams method according to described in section 3.2. We use the following definitions

$$\begin{aligned}
\Delta &:= \frac{T}{M}, \quad t_k := k \Delta, \quad k = 0, \dots, M, \quad \text{abs } \xi := 1 + |\xi|, \\
\tilde{h}(\xi, t) &:= \frac{h(\xi, t)}{1 + |\xi|}, \quad \tilde{h}_{\text{as}}(\xi, t) := \frac{-\frac{1}{2}(\xi^2 + i\xi)}{1 + |\xi|} \frac{t^\alpha}{\Gamma(\alpha + 1)}, \\
F(\xi, h) &:= -\frac{1}{2}(\xi^2 + i\xi) + \gamma (i\xi\rho\nu - 1) h + \frac{(\gamma\nu)^2}{2} h^2, \\
\tilde{F}_{\text{as1}}(\xi, \tilde{h}_{\text{as}}, \tilde{h}_1) &:= \gamma (i\xi\rho\nu - 1) (\tilde{h}_{\text{as}} + \tilde{h}_1) + (1 + |\xi|) \frac{(\gamma\nu)^2}{2} (\tilde{h}_{\text{as}} + \tilde{h}_1)^2.
\end{aligned}$$

The description, which can be found in the panel on the next page, is provided for illustration purposes only and does not include any optimizations or parallelizations.

Algorithm 1 Rough Heston CF via Fractional Adams – BL modification

Require: $\alpha \in (0, 1)$, $\gamma > 0$, $\theta > 0$, $\rho \in (-1, 1)$, $\nu > 0$, $v_0 > 0$, maturity T , steps M , Picard iterations n , frequency grid $\{\xi_m\}_{m=1}^N$

- 1: $\Delta \leftarrow T/M$; $t_k \leftarrow k \Delta$ for $k = 0, \dots, M$
- 2: **function** $a_{\text{unif}}(\alpha, \Delta, k)$ returns Adams weights $\{a_{j,k+1}\}_{j=0}^k$ for uniform grid
- 3: $r \leftarrow \Delta^\alpha / \Gamma(\alpha + 2)$ ▷ $r = a_{k+1,k+1}$ on a uniform grid
- 4: **for all** ξ in grid **do**
- 5: $\text{abs } \xi \leftarrow 1 + |\xi|$
- 6: **for** $k = 0, \dots, M$ **do**
- 7: $\tilde{h}_{\text{as}}(\xi, t_k) \leftarrow \frac{-\frac{1}{2}(\xi^2 + i\xi)}{\text{abs } \xi} \frac{t_k^\alpha}{\Gamma(\alpha + 1)}$
- 8: $\tilde{h}_1(\xi, t_0) \leftarrow 0$
- 9: $FF(\xi, 0) \leftarrow \tilde{F}_{\text{as1}}(\xi, \tilde{h}_{\text{as}}(\xi, t_0), \tilde{h}_1(\xi, t_0))$
- 10: **end for**
- 11: **for** $k = 0, \dots, M - 1$ **do**
- 12: $a_{0:k,k+1} \leftarrow a_{\text{unif}}(\alpha, \Delta, k)$ ▷ vector of weights $[a_{0,k+1}, \dots, a_{k,k+1}]^\top$
- 13: **for all** ξ in grid **do** ▷ predictor
- 14: $\tilde{h}_0(\xi) \leftarrow \sum_{j=0}^k a_{j,k+1} FF(\xi, j)$
- 15: $z \leftarrow \tilde{h}_0(\xi) + r \tilde{F}_{\text{as1}}(\xi, \tilde{h}_{\text{as}}(\xi, t_{k+1}), \tilde{h}_1(\xi, t_k))$ ▷ initial guess
- 16: **for** $m = 1, \dots, n$ **do** ▷ corrector
- 17: $z \leftarrow \tilde{h}_0(\xi) + r \tilde{F}_{\text{as1}}(\xi, \tilde{h}_{\text{as}}(\xi, t_{k+1}), z)$
- 18: $\tilde{h}_1(\xi, t_{k+1}) \leftarrow z$
- 19: $FF(\xi, k+1) \leftarrow \tilde{F}_{\text{as1}}(\xi, \tilde{h}_{\text{as}}(\xi, t_{k+1}), \tilde{h}_1(\xi, t_{k+1}))$ ▷ cache for next step
- 20: **end for**
- 21: **for all** ξ in grid **do** ▷ recover unscaled h on nodes
- 22: **for** $k = 0, \dots, M$ **do**
- 23: $\hat{h}(\xi, t_k) \leftarrow (1 + |\xi|) (\tilde{h}_{\text{as}}(\xi, t_k) + \tilde{h}_1(\xi, t_k))$
- 24: $G_k(\xi) \leftarrow \gamma \theta \hat{h}(\xi, t_k) + v_0 F(\xi, \hat{h}(\xi, t_k))$
- 25: $I(\xi) \leftarrow \Delta \left(\frac{1}{2} G_0(\xi) + \sum_{k=1}^{M-1} G_k(\xi) + \frac{1}{2} G_M(\xi) \right)$ ▷ trapezoid rule
- 26: $\Phi(\xi, T) \leftarrow \exp(I(\xi))$
- 27: **end for**

Ensure: $\{\Phi(\xi_m, T)\}_{m=1}^N$

APPENDIX C. BENCHMARK PRICING ALGORITHM

For a given pricing configuration X , i.e. a set of model parameters, option strike and expiry, and underlying spot level, the numerical parameters of the pricing algorithm are the ω in the definition of the sinh-acceleration (the slope of the asymptote of the deformed contour in the right half-plane), the number of discretization time steps M , the number of iterations n in the modified Adams method (cf. Remark 3.3), the mesh ζ and the number of terms N in the simplified trapezoid rule (see Section 4.1). Of all these, ω plays a special role since its choice determines the contour of integration along which the characteristic function is calculated, and hence determines the value of all other parameters. In addition, while it is clear that lower values of M , N and n , as well as higher values of ζ , correspond to lower CPU times, and decreasing accuracy, there is no such monotonic dependency on ω for either. Therefore, for the

calculation of the “best” ω , an optimization needs to be used to maximise pricing accuracy. We will use an objective function of ω , $F(\omega; X)$, which decreases for increasing pricing accuracy. For each configuration X , we evaluate the objective function $F(\omega; X)$ over a discrete grid¹³ $\Omega = \{\omega_1, \omega_2, \dots, \omega_m\}$. Let

$$\omega^{(0)} := \arg \min_{\omega_j \in \Omega} F(\omega_j; X)$$

denote the grid point that minimizes $F(\cdot; X)$. This value $\omega^{(0)}$ is used as the initial guess for a one-dimensional Nelder–Mead optimization, which yields a refined estimate ω_{best} . We record both ω_{best} and the associated pricing results for subsequent analysis and for training of the machine learning models.

C.1. Choice of ω grid. We give preference to values of ω that are small in absolute value, e.g., for the $\omega > 0$ strip case, $\omega \leq 0.2$, since such choices of ω tend to result in smaller M . Therefore we take $m = 10$ and $\Omega = \{\omega_1, \omega_2, \dots, \omega_{10}\}$, with¹⁴ $\omega_1 = 0.002$, $\omega_6 = 0.2$, $\omega_{10} = \pi/4 - 0.05$, with the intermediate points ω_2 to ω_5 , and ω_7 to ω_9 , equally spaced between ω_1 and ω_6 , and between ω_7 and ω_{10} , respectively. During the optimisation, we will let ω vary, in the $\omega > 0$ strip case, between a small nonzero value $\omega_0 = 0.0001$ and $\omega_{11} = \pi/4 - 0.0001$.

C.2. Calculation of $F(\omega; X)$. For each $\omega \in \Omega$, we calculate $F(\omega; X)$ as follows. First, if it has not already been calculated, we calculate the benchmark price $V_{LL}(T, K)$ corresponding to $\omega = 0$, i.e., after the sinh transformation, by integrating along the line $\text{Im } \xi = -1/2$ in Fourier space, which is the analogue of the Lewis–Lipton formula. This is done using the procedure in section C.3 below.

Then, for each $\omega \in \Omega$, we calculate $V(\omega; T, K)$, by using the same procedure with this value of ω . The value of $F(\omega)$ is calculated as

$$(C.1) \quad F(\omega) = (V_{LL} - V(\omega))^2,$$

C.3. Calculation of the benchmark prices $V(T, K; \omega)$. For each value of ω , including $\omega = 0$, we use the following algorithm.

1. We calculate the parameters ω_1 and b of the sinh-deformation and the mesh ζ according to the recommendations in section 4.8, where, for the put case, we take $\mu_+ = 1$, $\mu_- = 0$, $\gamma_{\pm} = \pm\pi/4$, $d = 0.9 \cdot \min(\gamma_+ - \omega, \omega - \gamma_-)$. We set $\zeta = 2\pi d / \log(100/\epsilon)$, where $\epsilon = 10^{-16}$ is our error tolerance.
2. We use the ad-hoc procedure described in Section 4.9 to calculate the truncation parameter $\Lambda = N\zeta$. Set $M = 1000$.
3. Calculate an initial price V_0 using the procedure in section 4.8, with $n = 2$.
4. In a loop $j = 1, 2, \dots, 10$, we check if the value of V_0 diverges, since the ad hoc recommendation at point 2 often results in too large values of Λ , which can cause division-by-zero errors in numerical calculations. In that case, we replace $\Lambda \mapsto 0.8 \cdot \Lambda$ and re-price.
5. Fix a tolerance $\epsilon_V = V_0/10000$.

¹³Here ω_1 is not to be confused with the parameter denoted with the same notation in the sinh-conformal map (cf. eq. (1.2)).

¹⁴See Section C.4 regarding the choice of ω_{10} .

6. Search for n . In a similar loop, calculate a new price V_1 and, while $|V_1 - V_0| \geq \epsilon_V$, and V_1 does not diverge, increase $n \mapsto n + 1$ and set V_1 equal to the old price V_0 . If $\omega = 0$, then we take the last n , since this value of ω is used to calculate V_{LL} , otherwise we reduce n by 1. In almost all cases, for $\omega \neq 0$, $n = 2$ is used.
7. Search for M . We use a similar loop to increase M , if needed, by a factor $\kappa_M = 1.5$ each time, up to a maximum of 4000 for the calculation of V_{LL} and 2500 otherwise¹⁵.
8. Choice of ζ and Λ . We use similar loops, first for the mesh ζ (with factors $\kappa_\zeta = 0.5$ for the calculation of V_{LL} and 0.8 otherwise) and the truncation parameter Λ (with factors $\kappa_\Lambda = 1.2$ for the calculation of V_{LL} and 1.1 otherwise). Care must be taken to restore the previous value of Λ , i.e. $\Lambda \mapsto \Lambda/\kappa_\Lambda$, if division by zero error occurs.
9. If the loop over Λ resulted in its value being increased, then we carry out a last loop over ζ .
10. Since the algorithm above can result in too large a value for M , if $\omega \neq 0$ we use the following approach to check if M can be reduced.
 - a. In a loop, reduce M by a factor of $\kappa'_M = 0.8$, as long as $|V - V_{\text{previous}}|/V_{\text{previous}} < 10^{-5}$.
 - b. Take the last working value of M before the check failed.

C.4. Calculation of $\omega(X)$. We store the values of $F(\omega_j)$, $\omega_j \in \{\omega_1, \omega_2, \dots, \omega_{10}\}$ in a vector and pick

$$\omega^{(0)} := \arg \min_{\omega_j \in \Omega} F(\omega_j; X)$$

to be the starting point of a 1D Nelder-Mead optimisation¹⁶ with function tolerance $\epsilon_f = 0.001$, argument tolerance $\epsilon_\omega = \min(8 \cdot 10^{-4}, 2\omega^{(0)}/100)$, maximum number of iterations set to 20, and maximum number of objective function evaluations set to 30. Call ω_{best} the result of the optimisation.

After the optimization completes, we check:

- If $|V(\omega_{\text{best}}) - V_{LL}|/V_{LL} < 10^{-4}$, then we store, for the configuration X , the value of ω_{best} , the price $V(\omega_{\text{best}})$, and the other numerical settings.
- Otherwise, we take the following alternative value of ω

$$k_{\text{alt}} := \arg \max_{k \in \{0,1\}} |\omega_k - \omega_{\text{best}}|, \quad \omega^{(\text{alt})} := \omega_{k_{\text{alt}}},$$

i.e., out of the two “best omegas” in Ω , we pick the one that differs the most from ω_{best} . If $V(\omega^{(\text{alt})})$ passes a similar check w.r.t. V_{LL} , then we store $\omega^{(\text{alt})}$, as well as the corresponding price and numerical settings.

- If neither of the previous checks works, then we compare $V(\omega_{\text{best}})$ and $V(\omega^{(\text{alt})})$ against each other. This can be useful on rare occasions when V_{LL} converges very slowly and is difficult to calculate with high precision.
- Finally, if none of the previous checks work, then we return an error¹⁷.

¹⁵Larger values of M than 2500 are sometimes needed, of course, however those would make a practical computation very slow.

¹⁶Using `scipy.optimize.minimize`.

¹⁷In our experiments, this has never been observed to happen.

APPENDIX D. PRICING ALGORITHM FOR THE MARKOVIAN APPROXIMATION (BL2)

This appendix outlines the BL2 algorithm described in [7]. The procedure in Appendix F of [7] is used to calculate the weights and nodes of the Markovian approximation. The full description of the pricing algorithm is not provided in [7] after the node construction, but can be found in the Python code published by the authors on GitHub [24], specifically in the function `compute_Fourier_inversion`, in file `rHestonFourier.py`. This algorithm adaptively refines the parameters of the Riccati solver and the Fourier inversion routine in order to satisfy a prescribed error tolerance. In particular, it adjusts the number of time steps in the Riccati ODE solver (M), the truncation point of the Fourier integral (L), and the number of quadrature points used in the Fourier inversion (N). For clarity of presentation, the algorithm is written in plain text rather than in pseudocode.

1. **Inputs:**

- Maturity T
- An array of strikes
- Relative error tolerance ε
- Hurst parameter $H > 0$
- A pricing routine $\text{compute}(M, L, N)$, that returns a vector of prices or implied volatilities, denoted as σ . This always uses flat iFT with, in our notation, $\omega = 2$ for put options and $\omega = -2$ for calls.

2. **Initial parameter guess:** The numerical parameters are initialized based on the maturity and Hurst parameter.

$$L = 100 \cdot T^{-0.5+H}, \quad M = \text{int}(10 \cdot L), \quad N = \text{int}(8 \cdot L)$$

3. **Baseline calculation:** A first solution is computed.

$$\sigma^{(0)} \leftarrow \text{compute}(M, L, N)$$

4. **Initial error estimation:** The error is estimated by comparing the baseline solution to a coarser one. This error is used to determine if the adaptive loop is necessary.

$$\sigma^{\text{coarse}} \leftarrow \text{compute}(\text{int}(M/1.6), L/1.2, \text{int}(N/2))$$

$$\text{error} = \max_k \frac{|\sigma_k^{\text{coarse}} - \sigma_k^{(0)}|}{|\sigma_k^{(0)}|}$$

5. **Adaptive refinement loop:** The loop continues as long as the error is above the tolerance¹⁸ ε or if the solution $\sigma^{(k)}$ contains invalid numbers (NaN). Let $k = 0$.

While ($\text{error} > \varepsilon$ **or** ($\sigma^{(k)}$) contains NaN):

- Store current solution:** $\sigma^{\text{old}} \leftarrow \sigma^{(k)}$.
- Check for NaN values in the solution:**

- **Case 1: No NaN values in $\sigma^{(k)}$**

- Shrink Test for Riccati time steps (M):** Check if M can be reduced.

$$\sigma^{\text{test}} \leftarrow \text{compute}(\text{int}(M/1.8), L, N)$$

¹⁸For the calculations in Table 8, we used $\varepsilon = 10^{-3}$.

$$\text{error}_R = \max_k \frac{|\sigma_k^{\text{test}} - \sigma_k^{(k)}|}{|\sigma_k^{(k)}|},$$

where $\text{int}(\cdot)$ rounds to the nearest integer. If $\text{error}_R < \varepsilon/5$, then update $M \leftarrow \text{int}(M/1.6)$.

- ii. **Shrink Test for Fourier quadrature points (N):** Check if N can be reduced.

$$\sigma^{\text{test}} \leftarrow \text{compute}(M, L, \text{int}(N/2))$$

$$\text{error}_F = \max_k \frac{|\sigma_k^{\text{test}} - \sigma_k^{(k)}|}{|\sigma_k^{(k)}|}$$

If $\text{error}_F < \varepsilon/5$, then update $N \leftarrow \text{int}(N/1.8)$.

- iii. **Refine parameters:** Increase parameters based on the component-wise errors.

$$\begin{aligned} L &\leftarrow 1.4 \cdot L \\ M &\leftarrow \begin{cases} \text{int}(1.4 \cdot M), & \text{if } \text{error}_R < \varepsilon/2 \\ 2 \cdot M, & \text{otherwise} \end{cases} \\ N &\leftarrow \begin{cases} \text{int}(1.4 \cdot N), & \text{if } \text{error}_F < \varepsilon/2 \\ 2 \cdot N, & \text{otherwise} \end{cases} \end{aligned}$$

• **Case 2: $\sigma^{(k)}$ contains NaN values**

- i. Increase parameters as follows:

$$L \leftarrow 1.6 \cdot L, \quad N \leftarrow \text{int}(1.7 \cdot N), \quad M \leftarrow \text{int}(2.5 \cdot M)$$

- c. **Recompute Solution:** Calculate the new solution with the updated parameters

$$\sigma^{(k+1)} \leftarrow \text{compute}(M, L, N)$$

- d. **Update Error:** Calculate the new error by comparing the new and old solutions:

$$\text{error} \leftarrow \max_k \frac{|\sigma_k^{\text{old}} - \sigma_k^{(k+1)}|}{|\sigma_k^{(k+1)}|}$$

- e. **Increment:** $k \leftarrow k + 1$.

6. **Return:** The final converged solution $\sigma^{(k)}$ and the final error estimate.

TABLE 10. Dependence of implied volatilities (rounded) in the rough Heston model on the numerical scheme. Example in [32, Sect. 6.2]; parameters $\alpha = 0.6$, $\gamma = 2$, $\rho = -0.6$, $\theta = 0.025$, $\nu = 0.2$, $v_0 = 0.025$). Spot $S = 1$, maturity $T = 1/52$ years (1 week).

K	0.8	0.85	0.9	0.95	1	1.05	1.1	1.15	1.2
SINH	0.4269	0.3686	0.3039	0.2274	0.1280	0.1313	0.1687	0.2053	0.2053
iFT(0.25, 4096)	(*)	0.3390	0.3009	0.2269	0.1280	0.1260	(*)	(*)	(*)
FFT(0.25,4096)	(*)	(*)	0.3000	0.2270	0.1279	0.1263	(*)	(*)	(*)
iFT(0.125,9182)	0.4273	0.3687	0.3039	0.2274	0.1280	0.1313	0.1687	0.2236	(*)
FFT(0.125,9182)	(*)	0.3539	0.3030	0.2274	0.1280	0.1315	0.1694	0.2175	(*)

SINH - method of the present paper, $\omega = 0.2$ for puts, $\omega = -0.2$ for calls.

iFT(ζ, N): iFT with $\omega_1 = -0.5$ (Lewis-Lipton choice) and uniform grid, step ζ, N terms.

FFT(ζ, N): version of CM method based on FFT and interpolation, with $\omega_1 = -0.5$, step ζ, N terms.

(*): price outside the no-arbitrage bounds.

$\sigma_{IMP}(1.2)$ in SINH-line is unreliable because the absolute value of the OTM option price is smaller than 10^{-12} .

APPENDIX E. ADDITIONAL TABLES AND FIGURES

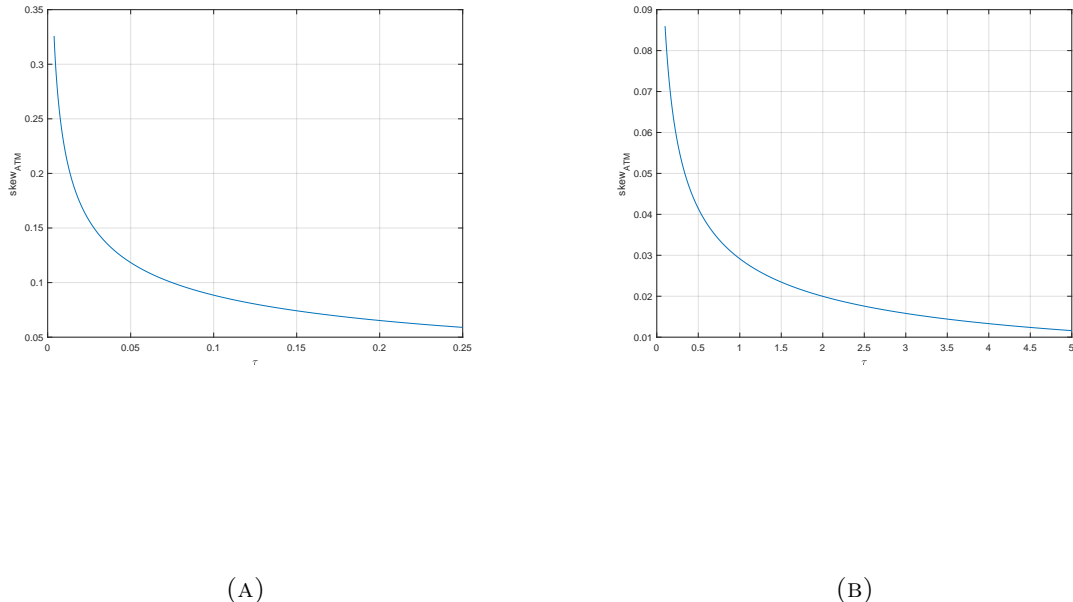


FIGURE 8. ATM skew; the parameters are in (1.3).

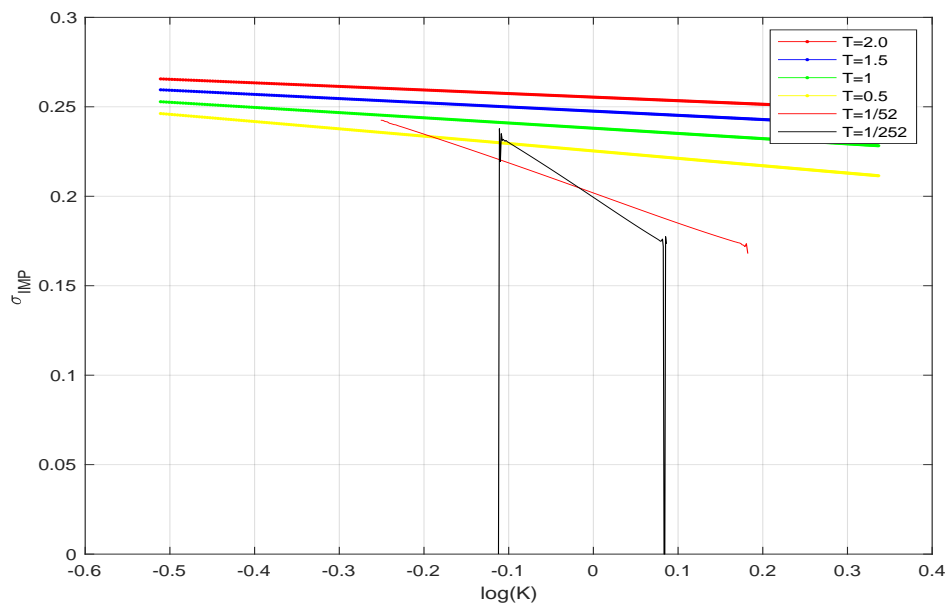


FIGURE 9. Implied volatility curves; the parameters are in (1.3). $\sigma_{IMP} = 0$ means that no-arbitrage condition is not satisfied.

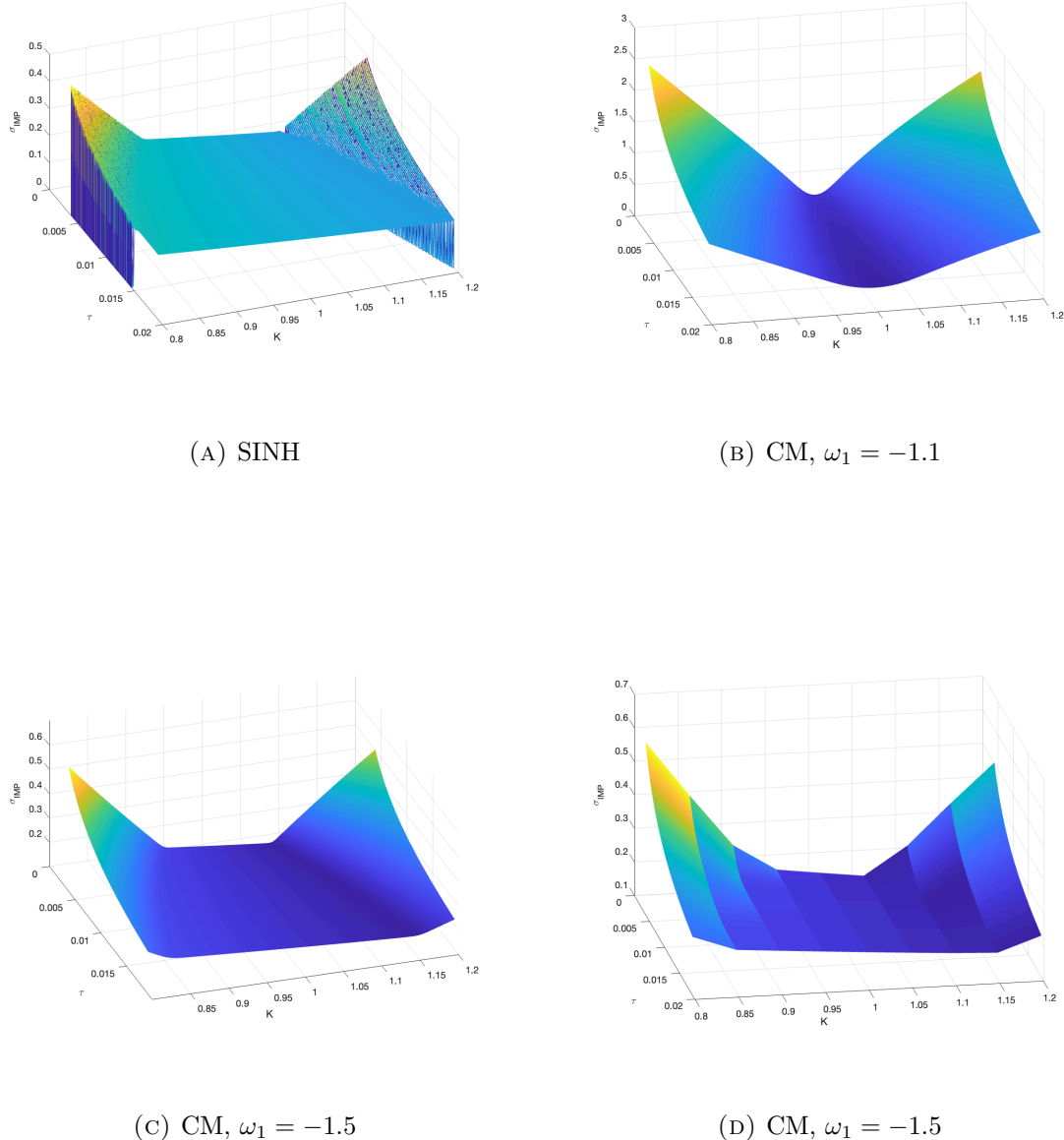


FIGURE 10. Implied volatility surfaces in the rough Heston model [34, Example 5.1], for time to maturity in the range (1 day, 1 week); spot $S_0 = 1$. If the price is outside the no-arbitrage bounds, σ_{IIMP} is set to 0. Panel (A): surface is calculated using the SINH-acceleration and the modified Adams method, the parameters are in (1.3). Irregular parts of the surface are where the OTM vanilla prices are smaller than E-10. Panels B-C: Flat iFT is used with $\zeta = 0.125$, $N = 8, 192$ and $\omega_1 = -1.1, -1.5, -1.5$, respectively, and the modified Adams method with $M = 2000$. Irregular parts of the surface are where the OTM vanilla price is smaller than E-06. Panel (D) shows the effect of the interpolation: implied volatilities are calculated at points of a sparse grid, in the result, the interpolated surface is higher than the one on Panel (C), and the smiles are more regular.

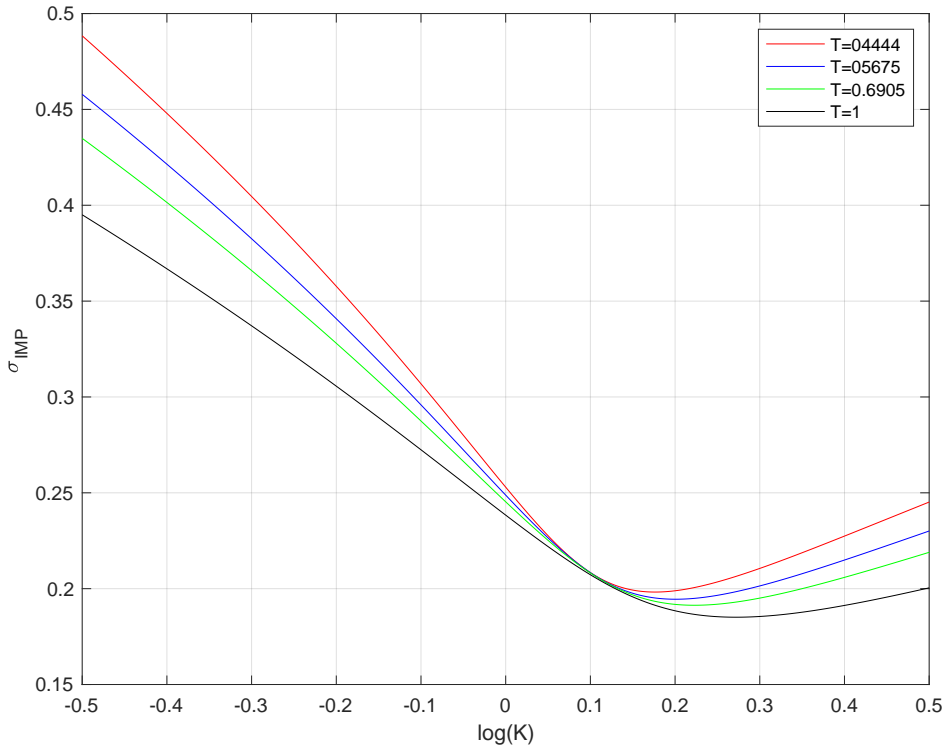


FIGURE 11. Correct implied volatility curves. The parameters $\alpha = 0.512$, $\gamma = 0.88$, $\rho = -0.7$, $\nu = 0.96$, $\theta = 0.016$, $v = 0.148$, are the result of calibration to the real data in [27, p.27]. The implied volatilities calculated using the Lewis and Adams methods and shown on Fig. 2.7 in [27] are somewhat different, in the tails especially. Note that on Fig. 2.7 in [27], the range of log-strikes is asymmetric, and depends on maturity: $\ln K \in [-0.3, 0.35]$ for maturities $T = 0.6905$ and $T = 1$, and $\ln K \in [-0.25, 0.35]$ for $T = 0.4444$ and $T = 0.5675$. A natural guess is that the results of calculations in the symmetric range $\ln K \in [-0.35, 0.35]$ are unsatisfactory.

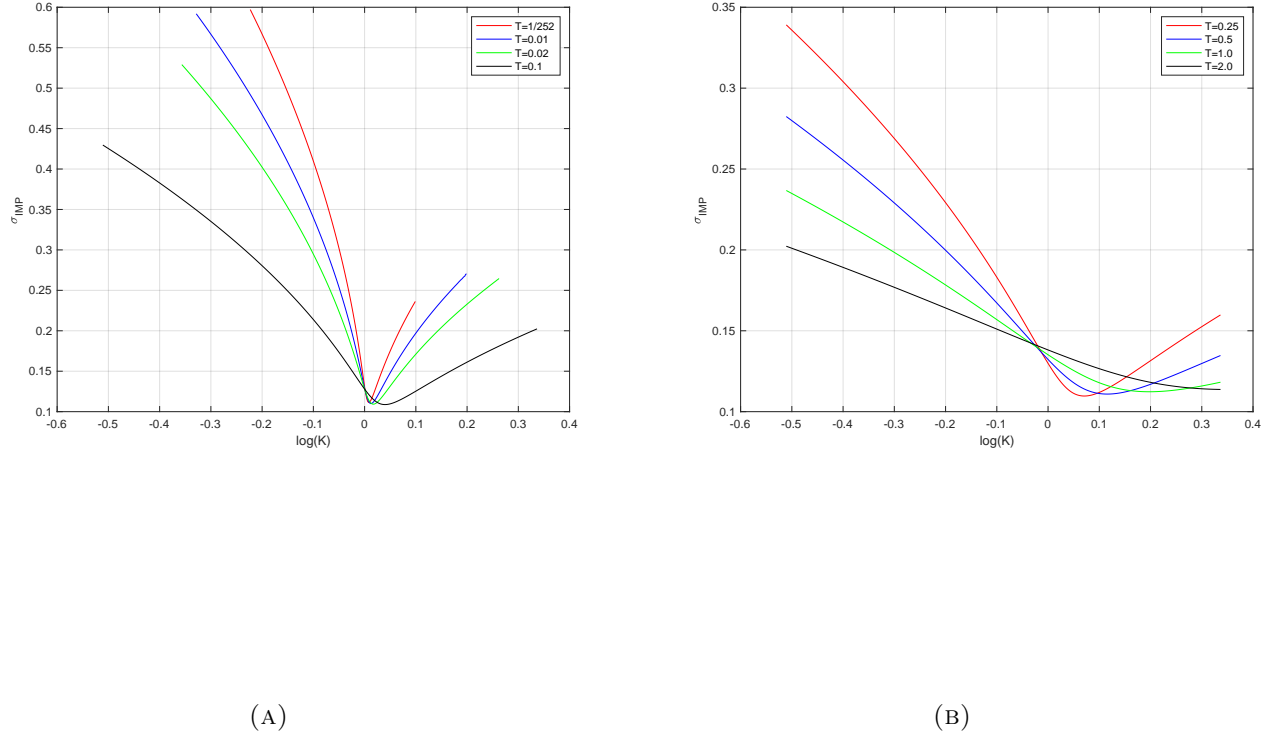


FIGURE 12. Correct implied volatility curves in the rough Heston model (Example in [32, Sect. 6.2]); parameters $\alpha = 0.6$, $\gamma = 2$, $\rho = -0.6$, $\theta = 0.025$, $\nu = 0.2$, $v_0 = 0.025$; $S_0 = 1$.

TABLE 11. Moderate maturities, spot $S_0 = 1$. Relative errors (rounded) of calculations of OTM and ATM puts ($K \leq 1$) and OTM calls ($K > 1$) in the rough Heston model with the parameters (1.3) and CPU time (in msec., the average over 1000 runs) for several numerical schemes.

$T = 2$										Time
K	0.80	0.85	0.90	0.95	1.00	1.05	1.10	1.15	1.20	
SINH	-1.5E-05	-1.2E-05	-9.6E-06	-8.0E-06	-6.7E-06	-7.9E-06	-9.3E-06	-1.1E-05	-1.3E-05	169.6
V_H	3.9E-06	-2.6E-06	1.4E-06	3.8E-06	1.3E-06	1.1E-06	-1.8E-06	1.6E-06	-3.1E-06	
Flat iFT-BM	-7.2E-06	-8.6E-06	-8.6E-06	-7.3E-06	-5.5E-06	-5.2E-06	-4.46E-06	-3.6E-06	-3.2E-06	97.7
Flat iFT	2.7E-07	-1.6E-06	-2.4E-06	-2.2E-06	-1.5E-06	-1.0E-06	-4.9E-08	1.0E-06	1.8E-06	661.5
Lewis 30	4.4E-06	-1.9E-07	-1.4E-06	-1.3E-06	-8.3E-07	-5.7E-07	-2.4E-07	8.5E-08	3.7E-07	400.8

SINH: $\omega_1 = -0.5$, $b = 0.769884522$, $\omega = 0$, $\zeta = 0.285754315$, $N = 12$, BL Modification with $M = 317$.

V_H : hybrid method of [25]

Flat iFT-BM: $\sigma_0 = 1$, $\omega_1 = -0.5$, $\zeta = 0.717626524$, $N = 16$, BL Modification with $M = 317$.

Flat FT: $\omega_1 = -0.5$, $\zeta = 0.109637386$, $N = 110$, BL Modification with $M = 317$.

Lewis 30: Lewis method and Gauss-Legendre quadrature with 30 terms, BL Modification with $M = 317$.

CPU time is for the evaluation of $\Phi(\xi_k, \tau_m)$, for $k = 0, 1, \dots, N$, $m = 1, \dots, 317$.

Flat iFT-BM is used with the parallelization w.r.t. ξ .

SINH, Flat iFT and Lewis method are used without the parallelization w.r.t. ξ .

For the Lewis method, the nodes and weights are precalculated.

For V_H , the CPU time is in the range 593-667 msec. per strike.

$T = 1$											Time
	0.80	0.85	0.90	0.95	1.00	1.05	1.10	1.15	1.20		
SINH	-2.1E-05	-1.5E-05	-1.1E-05	-8.0E-06	-6.1E-06	-7.8E-06	-1.0E-05	-1.3E-05	-1.7E-05	295.6	
V_H	-1.8E-05	9.9E-06	-4.5E-06	7.2E-06	-1.9E-06	-6.7E-07	-1.1E-05	-1.0E-05	-1.9E-05		
Flat iFT-BM	9.3E-06	3.5E-06	-2.1E-06	-3.3E-06	-1.6E-06	7.3E-07	4.1E-06	6.0E-06	3.6E-06	102.9	
Flat iFT	1.1E-05	3.6E-06	-3.0E-06	-4.0E-06	-1.8E-06	1.1E-06	5.1E-06	7.2E-06	4.14E-06	980.8	
Lewis 30	1.2E-04	3.4E-05	-1.706	-7.7E-06	-5.1E-06	-3.4E-06	-7.4E-07	2.3E-06	5.8E-06	144.1	

SINH: $\omega_1 = -0.5$, $b = 0.769884522$, $\omega = 0$, $\zeta = 0.285754315$, $N = 14$, BL Modification with $M = 399$.

V_H : hybrid method of [25]

Flat iFT-BM: $\sigma_0 = 0.5$, $\omega_1 = -0.5$, $\zeta = 0.717626524$, $N = 22$, BL Modification with $M = 317$.

Flat FT: $\omega_1 = -0.5$, $\zeta = 0.0877$, $N = 200$, BL Modification with $M = 317$.

Lewis 30: Lewis method and Gauss-Legendre quadrature with 30 terms, BL Modification with $M = 317$.

For V_H , the CPU time is in the range 548-582 msec. per strike.

$T = 0.5$											Time
	0.80	0.85	0.90	0.95	1.00	1.05	1.10	1.15	1.20		
SINH	4.4E-05	5.1E-05	-7.9E-06	-1.9E-05	-2.7E-06	-3.5E-06	-37E-06	-5.1E-06	-8.6E-06	329.6	
V_H	3.3E-05	-2.0E-05	2.8E-06	-5.2E-06	-8.6E-06	-1.7E-06	-1.9E-05	7.7E-06	-4.3E-05		
Flat iFT-BM	4.4E-05	5.1E-05	-7.9E-06	-1.9E-05	-2.7E-06	1.8E-05	2.6E-05	-1.2E-05	-9.4E-05	107.3	
Flat iFT	-1.4E-05	1.0E-05	2.1E-06	-4.4E-06	-2.1E-06	2.5E-06	6.2E-06	-1.73E-06	-2.2E-05	1,192.3	
Lewis 35	7.7E-04	1.2E-04	-3.2E-05	-1.9E-05	-2.9E-06	1.5E-06	2.2E-06	5.8E-06	2.9E-05	465.4	

SINH: $\omega_1 = -0.5$, $b = 0.769884522$, $\omega = 0$, $\zeta = 0.1836992027$, $N = 23$, BL Modification with $M = 317$.

V_H : hybrid method of [25]

Flat iFT-BM: $\sigma_0 = 0.5$, $\omega_1 = -0.5$, $\zeta = 0.789389176$, $N = 30$, BL Modification with $M = 317$.

Flat FT: $\omega_1 = -0.5$, $\zeta = 0.0877$, $N = 200$, BL Modification with $M = 317$.

Lewis 35: Lewis method and Gauss-Legendre quadrature with 35 terms, BL Modification with $M = 317$.

For V_H , the CPU time is in the range 666-689 msec. per strike.

TABLE 12. Short maturities, spot $S_0 = 1$. Relative errors (rounded) of calculations of OTM and ATM puts ($K \leq 1$) and OTM calls ($K > 1$) in the rough Heston model with the parameters (1.3) for several numerical scheme and CPU time (in msec., the average over 1000 runs).

$T = 1/12$	K	0.80	0.85	0.90	0.95	1.00	1.05	1.10	1.15	1.20	Time
SINH		1.4E-05	-2.1E-04	-1.2E-05	-2.9E-07	-1.8E-06	-5.8E-07	5.8E-06	-1.3E-04	2.9E-03	415.7
V_H		-0.057	-0.0018	3.5E-04	-8.7E-05	-3.3E-05	-3.3E-05	-1.35E-05	-2.4E-04	7.8E-03	
Flat iFT-BM	-0.092	1.5E-03	1.2E-04	-5.0E-05	1.6E-05	-3.4E-05	-1.1E-04	5.2E-04	-0.15	133.3	
Flat iFT	-5.6	0.13	0.017	-0.0083	0.0024	-9.4E-04	-0.047	0.42	2.7	2,341.2	
Lewis 80	0.045	-0.0073	1.7E-04	-5.8E-06	6.9E-08	-3.8E-07	4.0E-06	-3.3E-05	-0.013	1,062.3	

SINH: $\omega_1 = -0.5$, $b = 0.769884522$, $\omega = 0$, $\zeta = 0.1836992027$, $N = 28$, BL Modification with $M = 317$.

V_H : hybrid method of [25]

Flat iFT-BM: $\sigma_0 = 0.5$, $\omega_1 = -0.5$, $\zeta = 0.717626524$, $N = 80$, BL Modification with $M = 317$.

Flat FT: $\omega_1 = -0.5$, $\zeta = 0.0877$, $N = 450$, BL Modification with $M = 317$.

Lewis 80: Lewis method and Gauss-Legendre quadrature with 80 terms, BL Modification with $M = 317$.

For V_H , the CPU time is in the range 410-423 msec. per strike.

$T = 1/52$	K	0.85	0.90	0.95	1.00	1.05	1.10	1.15	Time
SINH		-0.42	1.5E-03	-1.6E-05	-6.6E-06	-2.3E-04	-0.043	-205	154.8
V_H		(**)	0.013	0.085	0.016	0.096	0.32	0.82	
Flat iFT-BM	26.5	2.8E-03	-1.1E-04	-9.4E-07	1.3E-04	0.075	1,030	339.3	
Flat iFT	1,167	0.71	3.9E-04	1.5E-04	1.7E-03	-1.7	-49,413	1,664.2	
Lewis 100	25,177	1.2	3.5E-04	4.3E-07	6.3E-05	0.60	-119,127	187.8	

At $K = 0.8$ and $K = 1.2$, the prices of OTM options are smaller than 10^{-12} , and the benchmark prices cannot be calculated using double precision arithmetic.

SINH, puts: $\omega_1 = 0.325762041$, $b = 1.014615984$, $\omega = 0.2$, $\zeta = 0.145086905$, $N = 38$, BL Modification with $M = 100$

SINH, calls: $\omega_1 = -1.325762041$, $b = 1.014615984$, $\omega = -0.2$, $\zeta = 0.145086905$, $N = 38$, BL Modification with $M = 100$.

V_H : hybrid method of [25]; (**): the call price in [25] implies that the price of the put is 0.

Flat iFT-BM: $\sigma_0 = 0.5$, $\omega_1 = -0.5$, $\zeta = 0.717626524$, $N = 200$, BL Modification with $M = 100$.

Flat FT: $\omega_1 = -0.5$, $\zeta = 0.07309159$, $N = 1500$, BL Modification with $M = 100$.

Lewis 100: Lewis method and Gauss-Legendre quadrature with 100 terms, BL Modification with $M = 100$.

The order of the errors of Flat iFT-BM, Flat FT and Lewis 100 does not decrease if N increases further.

For V_H , the CPU time is in the range 125-164 msec. per strike.

$T = 1/252$	K	0.95	1.00	1.05	Time
SINH		-2.7E-03	4.7E-07	9.0E-03	212.1
V_H		11.2	1.7E-04	18.3	
Flat iFT-BM		-0.51	1.E-04	18.8	557.8
Flat iFT		-17.8	3.1E-03	-370	1,664.2
Lewis 100		6.3	-2.2E-05	270	190.1

At $K = 0.80, 0.85, 0.90$ and $K = 1.10, 1.15, 1.20$, the prices of OTM options are smaller than 10^{-12} , and the benchmark prices cannot be calculated accurately using double precision arithmetic.

SINH, puts: $\omega_1 = 0.325762041$, $b = 1.014615984$, $\omega = 0.2$, $\zeta = 0.145086905$, $N = 46$, BL Modification with $M = 100$.

SINH, calls: $\omega_1 = -1.325762041$, $b = 1.014615984$, $\omega = -0.2$, $\zeta = 0.145086905$, $N = 46$, BL Modification with $M = 100$.

V_H : hybrid method of [25].

Flat iFT-BM: $\sigma_0 = 0.5$, $\omega_1 = -0.5$, $\zeta = 0.717626524$, $N = 350$, BL Modification with $M = 100$.

Flat FT: $\omega_1 = -0.5$, $\zeta = 0.07309159$, $N = 1500$, BL Modification with $M = 100$.

Lewis 100: Lewis method and Gauss-Legendre quadrature with $N = 100$ terms, BL Modification with $M = 100$.

The order of the errors of Flat iFT-BM, Flat FT and Lewis does not decrease if N increases further.

For V_H , the CPU time is in the range 154-196 msec. per strike.

TABLE 13. Implied volatilities for options of short maturities in Table 12.

$T = 1/12$										
K	0.80	0.85	0.90	0.95	1.00	1.05	1.10	1.15	1.20	
BB	0.2280	0.2226	0.2173	0.2123	0.2075	0.2030	0.1986	0.1945	0.1907	
SINH	0.2280	0.2225	0.2173	0.2123	0.2075	0.2030	0.1986	0.1945	0.1907	
V_H	0.2271	0.2225	0.2173	0.2123	0.2075	0.2030	0.1986	0.1944	0.1907	
Flat iFT-BM	0.2265	0.2226	0.2173	0.2123	0.2075	0.2030	0.1986	0.1947	0.1884	
Flat iFT	(**)	0.2257	0.2181	0.2116	0.2080	0.2030	0.1968	0.2029	0.2116	
Lewis 100	0.2243	0.2226	0.2173	0.2123	0.2075	0.2030	0.1986	0.1945	0.1911	
$T = 1/52$										
K	0.8	0.85	0.90	0.95	1.00	1.05	1.10	1.15	1.20	
BB	0.2383	0.2288	0.2195	0.2105	0.2018	0.1935	0.1857	0.1786	0.1737	
SINH	0.2450	0.2288	0.2195	0.2105	0.2018	0.1935	0.1857	0.1786	0.1703	
V_H	(**)	(**)	0.2197	0.2138	0.2051	0.1968	0.1889	0.1818	0.1843	
Flat iFT-BM	(*)	0.2600	0.2196	0.2105	0.2018	0.1935	0.1866	0.2291	0.2929	
Flat iFT	0.4029	0.3147	0.2280	0.2107	0.2019	0.1936	(*)	(*)	0.3071	
Lewis 100	0.5883	0.3928	0.2321	0.2106	0.2018	0.1935	0.1913	(*)	(*)	
$T = 1/252$										
K		0.95	1.00	1.05						
BB		0.2154	0.1994	0.1841						
SINH		0.2154	0.1994	0.1841						
V_H		0.2552	0.1994	0.2174						
Flat iFT-BM		0.2068	0.1994	0.2178						
Flat iFT		(*)	0.2000	(*)						
Lewis 100		0.2456	0.1994	0.2661						

BB: benchmark.

(*): the price outside the no-arbitrage bounds.

(**): the put price is smaller than 10^{-12} .TABLE 14. Calculation of put price using the conformal bootstrap principle. The first ten terms in the truncated infinite trapezoid rule for different deformations. Parameters of the rough Heston model are in (1.3). Spot $S_0 = 1$, strike $K = 0.8$.

A	B	C
0.0126901431392702	0.0120833046030836	-0.0501714124280455
0.0242986340385064	0.0231211186180477	-0.0979019237170768
0.0213606748407816	0.0202897147441772	-0.091265572010822
0.0172925461013434	0.0163928017598907	-0.0820545925250891
0.0128572463702778	0.0121840249842967	-0.0719647606426263
0.00860236532132357	0.00819835636016092	-0.0622003080137314
0.00481907034448851	0.00471166226701002	-0.0533833514890913
0.00161240610274295	0.00181184828931256	-0.0457144196494677
-0.00101555302680714	-0.000516884192064965	-0.0391624761289111
-0.00310798338760139	-0.0023350244083961	-0.0335980796640654

In all three cases, the BL Modification of the Adams method is used with $M = 1000$.In Cases A and B, the deformed contour is in the upper half-plane, and the sum of the terms shown is the put price V_{put} . A: $V_{put} = 0.00611179127528501$; B: $V_{put} = 0.00611179083570821$ In Case C, the deformed contour is the horizontal line $\{\text{Im } \xi = -0.5\}$, the sum of the terms shown is the covered call price, and the put price is obtained adding $K = 0.8$. $V_{put} = 0.00611179093246816$.

Parameters of the numerical scheme:

A: $\omega_1 = 0.429259757$, $b = 0.868680815$, $\omega = 0.1$, $\zeta = 0.100193684$, $N = 42$.B: $\omega_1 = 0.325762041$, $b = 1.014615984$, $\omega = 0.2$, $\zeta = 0.085575366$, $N = 47$.C: $\omega_1 = -0.5$, $b = 0.769884522$, $\omega = 0$, $\zeta = 0.114812002$, $N = 41$.

TABLE 15. “Bad region in the parameters space”. Prices of OTM and ATM put and OTM call options of short maturity $T = 1/365$, $r = 0.1$, spot $S_0 = 1000$, in the KoBoL model of small order, with parameters $(\mu, c, \nu, \lambda_+, \lambda_-) = (0.1, 1, 0.5, 0.2, -1.2)$, and relative errors of SINH-, Gauss-Laguerre (GL) and Gauss-Kronrod (GK) quadratures w.r.t. V . N is the number of terms.

K	0.6	0.8	1	1.2	1.4	N
V	1.15596308274723	2.2769702099306	5.97763601818645	3.06782338691266	2.39427586598299	105-274-114
$SINH$	-7.22E-06	-4.33E-06	-1.90E-06	-3.96E-06	-5.38E-06	33-94-36
GL	1.86E-04	-5.05E-03	0.036	4.12E-03	9.53E-04	175
GK	1.45E-04	1.25E-05	-2.14E-05	1.59E-05	-2.70E-05	

Relative errors of the benchmark prices are smaller than $E - 13$, and defined as differences of prices calculated with $\omega = \pm\pi/4$ and $\omega = \pm\pi/8$, following the general prescription with the error tolerance $\epsilon = E - 15$ and dividing (resp., multiplying) ζ and Λ by 1.4.

$SINH$ - calculated for $\omega = \pm\pi/4$, following the general prescription for $\epsilon = E - 07$

TABLE 16. “Good region in the parameters space”. Prices of OTM and ATM put and OTM call options of short maturity $T = 1$, $r = 0.1$, spot $S_0 = 1000$, in the KoBoL model of large order, with parameters $(\mu, c, \nu, \lambda_+, \lambda_-) = (0.1, 1, 0.5, 0.2, -1.2)$, and relative errors of SINH-, Gauss-Laguerre (GL) and Gauss-Kronrod (GK) quadratures w.r.t. V . N is the number of terms.

K	0.6	0.8	1	1.2	1.4	N
V	326.631884432011	469.61080845886	618.758920614544	686.548810890079	662.549963116958	53-54
$SINH$	0	0	0	0	-1.55E-12	38-39
GL	2.86E-11	2.22E-11	1.86E-11	1.84E-11	2.07E-11	175
GK	1.15E-14	-3.51E-15	-6.61E-15	-6.62E-15	-5.15E-15	

Relative errors of the benchmark prices are 0 (calculated in Matlab with double precision arithmetic), and defined as differences of prices calculated with $\omega = \pm\pi/4$ and $\omega = \pm\pi/8$, following the general prescription with the error tolerance $\epsilon = E - 15$ and dividing (resp., multiplying) ζ and Λ by 1.4.

$SINH$ - calculated for $\omega = \pm\pi/4$, following the general prescription for $\epsilon = E - 15$